



1

2

3

The IceCube Data Acquisition System: Signal Capture, Digitization, and Timestamping

4 R. Abbasi^t, M. Ackermann^{af}, J. Adams^k, M. Ahlers^y, J. Ahrens^u, K. Andeen^t, J. Auffenberg^{ac}, X. Bai^w, M.
 5 Baker^t, S. W. Barwick^p, R. Bay^e, J. L. Bazo Alba^{af}, K. Beattie^f, T. Becka^u, J. K. Becker^m, K.-H. Becker^{ae}, P.
 6 Berghaus^t, D. Berley^l, E. Bernardini^{af}, D. Bertrand^h, D. Z. Besson^t, B. Bingham^f, E. Blaufuss^l, D. J.
 7 Boersma^t, C. Boehm^z, J. Bolmont^{af}, S. Böser^{af}, O. Botner^{ac}, J. Braun^t, D. Breder^{ae}, T. Burgess^z, W. Carithers
 8 ^f, T. Castermans^v, H. Chen^f, D. Chirkin^t, B. Christy^l, J. Clem^w, D. F. Cowen^{ab,aa}, M. V. D'Agostino^e, M.
 9 Danninger^k, A. Davour^{ac}, C. T. Day^f, O. Depaeppeⁱ, C. De Clercqⁱ, L. Demirörs^q, F. Descampsⁿ, P. Desiati^t, G.
 10 de Vries-Uiterweerdⁿ, T. DeYoung^{ab}, J. C. Diaz-Velez^t, J. Dreyer^m, J. P. Dumm^t, M. R. Duvoort^{ad}, W. R.
 11 Edwards^f, R. Ehrlich^l, J. Eisch^t, R. W. Ellsworth^l, O. Engdegård^{ac}, S. Euler^a, P. A. Evenson^w, O. Fadiran^c, A.
 12 R. Fazely^d, T. Feuselsⁿ, K. Filimonov^e, C. Finley^t, M. M. Foerster^{ab}, B. D. Fox^{ab}, A. Franckowiak^g, R. Franke
 13 ^{af}, T. K. Gaisser^w, J. Gallagher^s, R. Ganugapati^t, L. Gerhardt^f, L. Gladstone^t, D. Glowacki^t, A. Goldschmidt^f,
 14 J. A. Goodman^l, R. Gozzini^u, D. Grant^{ab}, T. Griesel^u, A. Groß^{o,k}, S. Grullon^t, R. M. Gunasingha^d, M. Gurtner
 15 ^{ae}, C. Ha^{ab}, A. Hallgren^{ac}, F. Halzen^t, K. Han^k, K. Hanson^t, R. Hardtke^y, Y. Hasegawa^j, J. Haugen^t, D. Hays^f,
 16 J. Heise^{ad}, K. Helbing^{ae}, M. Hellwig^u, P. Herquet^v, S. Hickford^k, G. C. Hill^t, J. Hodges^t, K. D. Hoffman^l, K.
 17 Hoshina^t, D. Hubertⁱ, W. Huelsnitz^l, B. Hughey^t, J.-P. Hülß^a, P. O. Hulth^z, K. Hultqvist^z, S. Hussain^w, R. L.
 18 Imlay^d, M. Inaba^j, A. Ishihara^j, J. Jacobsen^t, G. S. Japaridze^c, H. Johansson^z, A. Jones^f, J. M. Joseph^f, K.-H.
 19 Kampert^{ae}, A. Kappes^{t,1}, T. Karg^{ae}, A. Karle^t, H. Kawai^j, J. L. Kelley^t, J. Kiryluk^{f,e}, F. Kislak^{af}, S. R. Klein^{f,e},
 20 S. Kleinfelder^f, S. Klepser^{af}, G. Kohlen^v, H. Kolanoski^g, L. Köpke^u, M. Kowalski^g, T. Kowarik^u, M.
 21 Krasberg^t, K. Kuehn^p, E. Kujawski^f, T. Kuwabara^w, M. Labare^h, K. Laihem^a, H. Landsman^t, R. Lauer^{af}, A.
 22 Landrie^t, H. Leich^{af}, D. Leier^m, C. Lewis^t, A. Lucke^g, J. Ludvig^f, J. Lundberg^{ac}, J. Lünemann^m, J. Madsen^y,
 23 R. Maruyama^t, K. Mase^j, H. S. Matis^{f,2}, C. P. McParland^f, K. Meagher^l, A. Meli^m, M. Merck^t, T. Messarius^m,
 24 P. Mészáros^{ab,aa}, R. H. Minor^f, H. Miyamoto^j, A. Mohr^g, A. Mokhtarani^f, T. Montaruli^{t,3}, R. Morse^t, S. M.

¹ On leave of absence from Universität Erlangen-Nürnberg, Physikalisches Institut, D-91058, Erlangen, Germany.

² Corresponding author. Tel.: +1-510-486-5031; fax: +1-510-486-4818; e-mail: hsmatis@lbl.gov.

³ On leave of absence from Università di Bari and INFN, Dipartimento di Fisica, I-70126, Bari, Italy.

25 Movit ^{aa}, K. München ^m, A. Muratas ^f, R. Nahnauer ^{af}, J. W. Nam ^p, P. Nießen ^w, D. R. Nygren ^f, S. Odrowski ^o, A.
 26 Olivas ^l, M. Olivo ^{ac}, M. Ono ^j, S. Panknin ^g, S. Patton ^f, C. Pérez de los Heros ^{ac}, J. Petrovic ^h, A. Piegsa ^u, D.
 27 Pieloth ^{af}, A. C. Pohl ^{ac,4}, R. Porrata ^e, N. Potthoff ^{ae}, J. Pretz ^l, P. B. Price ^e, G. T. Przybylski ^f, K. Rawlins ^b, S.
 28 Razzaque ^{ab,aa}, P. Redl ^l, E. Resconi ^o, W. Rhode ^m, M. Ribordy ^q, A. Rizzo ⁱ, W. J. Robbins ^{ab}, J. P. Rodrigues ^t,
 29 P. Roth ^l, F. Rothmaier ^u, C. Rott ^{ab,5}, C. Roucelle ^{f,c}, D. Rutledge ^{ab}, D. Ryckbosch ⁿ, H.-G. Sander ^u, S. Sarkar ^x,
 30 K. Satalecka ^{af}, P. Sandstrom ^t, S. Schlenstedt ^{af}, T. Schmidt ^l, D. Schneider ^t, O. Schulz ^o, D. Seckel ^w, B.
 31 Semburg ^{ac}, S. H. Seo ^z, Y. Sestayo ^o, S. Seunarine ^k, A. Silvestri ^p, A. J. Smith ^l, C. Song ^t, J. E. Sopher ^f, G. M.
 32 Spiczak ^y, C. Spiering ^{af}, T. Stanev ^w, T. Stezelberger ^f, R. G. Stokstad ^f, M. C. Stoufer ^f, S. Stoyanov ^w, E. A.
 33 Strahler ^t, T. Straszheim ^l, K.-H. Sulanke ^{af}, G. W. Sullivan ^l, Q. Swillens ^h, I. Taboada ^{e,6}, O. Tarasova ^{af}, A. Tepe
 34 ^{ac}, S. Ter-Antonyan ^d, S. Tilav ^w, M. Tluczykont ^{af}, P. A. Toale ^{ab}, D. Tosi ^{af}, D. Turčan ^l, N. van Eijndhoven ^{ad}, J.
 35 Vandenbroucke ^e, A. Van Overloop ⁿ, V. Viscomi ^{ab}, C. Vogt ^a, B. Voigt ^{af}, C. Q. Vu ^f, D. Wahl ^t, C. Walck ^z, T.
 36 Waldenmaier ^w, H. Waldmann ^{af}, M. Walter ^{af}, C. Wendt ^t, S. Westerhof ^t, N. Whitehorn ^t, D. Wharton ^t, C. H.
 37 Wiebusch ^a, C. Wiedemann ^z, G. Wikström ^z, D. R. Williams ^{ab,7}, R. Wischniewski ^{af}, H. Wissing ^a, K. Woschnagg
 38 ^e, X. W. Xu ^d, G. Yodh ^p, S. Yoshida ^j
 39 (The IceCube Collaboration)

40 ^a*III Physikalisches Institut, RWTH Aachen University, D-52056 Aachen, Germany*

41 ^b*Dept. of Physics and Astronomy, University of Alaska Anchorage, 3211 Providence Dr., Anchorage, AK 99508, USA*

42 ^c*CTSPS, Clark-Atlanta University, Atlanta, GA 30314, USA*

43 ^d*Dept. of Physics, Southern University, Baton Rouge, LA 70813, USA*

44 ^e*Dept. of Physics, University of California, Berkeley, CA 94720, USA*

45 ^f*Lawrence Berkeley National Laboratory, Berkeley, CA 94720, USA*

46 ^g*Institut für Physik, Humboldt-Universität zu Berlin, D-12489 Berlin, Germany*

47 ^h*Université Libre de Bruxelles, Science Faculty CP230, B-1050 Brussels, Belgium*

48 ⁱ*Vrije Universiteit Brussel, Dienst ELEM, B-1050 Brussels, Belgium*

49 ^j*Dept. of Physics, Chiba University, Chiba 263-8522, Japan*

50 ^k*Dept. of Physics and Astronomy, University of Canterbury, Private Bag 4800, Christchurch, New Zealand*

51 ^l*Dept. of Physics, University of Maryland, College Park, MD 20742, USA*

52 ^m*Dept. of Physics, Universität Dortmund, D-44221 Dortmund, Germany*

⁴ Affiliated with School of Pure and Applied Natural Sciences, Kalmar University, S-39182 Kalmar, Sweden.

⁵ Currently at Dept. of Physics and Center for Cosmology and Astro-Particle Physics, The Ohio State University, Columbus, OH 43210, USA.

⁶ Currently at the School of Physics and Center for Relativistic Astrophysics, Georgia Institute of Technology, Atlanta, GA 30332, USA.

⁷ Currently at the Dept. of Physics and Astronomy, University of Alabama, Tuscaloosa, AL 35487, USA.

- 53 ⁿ Dept. of Subatomic and Radiation Physics, University of Gent, B-9000 Gent, Belgium
- 54 ^o Max-Planck-Institut für Kernphysik, D-69177 Heidelberg, Germany
- 55 ^p Dept. of Physics and Astronomy, University of California, Irvine, CA 92697, USA
- 56 ^q Laboratory for High Energy Physics, École Polytechnique Fédérale, CH-1015 Lausanne, Switzerland
- 57 ^r Dept. of Physics and Astronomy, University of Kansas, Lawrence, KS 66045, USA
- 58 ^s Dept. of Astronomy, University of Wisconsin, Madison, WI 53706, USA
- 59 ^t Dept. of Physics, University of Wisconsin, Madison, WI 53706, USA
- 60 ^u Institute of Physics, University of Mainz, Staudinger Weg 7, D-55099 Mainz, Germany
- 61 ^v University of Mons-Hainaut, 7000 Mons, Belgium
- 62 ^w Bartol Research Institute, University of Delaware, Newark, DE 19716, USA
- 63 ^x Dept. of Physics, University of Oxford, 1 Keble Road, Oxford OX1 3NP, UK
- 64 ^y Dept. of Physics, University of Wisconsin, River Falls, WI 54022, USA
- 65 ^z Dept. of Physics, Stockholm University, SE-10691 Stockholm, Sweden
- 66 ^{aa} Dept. of Astronomy and Astrophysics, Pennsylvania State University, University Park, PA 16802, USA
- 67 ^{ab} Dept. of Physics, Pennsylvania State University, University Park, PA 16802, USA
- 68 ^{ac} Division of High Energy Physics, Uppsala University, S-75121 Uppsala, Sweden
- 69 ^{ad} Dept. of Physics and Astronomy, Utrecht University/SRON, NL-3584 CC Utrecht, The Netherlands
- 70 ^{ae} Dept. of Physics, University of Wuppertal, D-42119 Wuppertal, Germany
- 71 ^{af} DESY, D-15735 Zeuthen, Germany
- 72 **Elsevier use only:** Received date here; revised date here; accepted date here

73 **Abstract**

74 IceCube is a km-scale neutrino observatory under construction at the South Pole with sensors both in the deep ice
75 (InIce) and on the surface (IceTop). The sensors, called Digital Optical Modules (DOMs), detect, digitize and
76 timestamp the signals from optical Cherenkov-radiation photons. The DOM Main Board (MB) data acquisition
77 subsystem is connected to the central DAQ in the IceCube Laboratory (ICL) by a single twisted copper wire-pair
78 and transmits packetized data on demand. Time calibration is maintained throughout the array by regular
79 transmission to the DOMs of precisely timed analog signals, synchronized to a central GPS-disciplined clock.
80 The design goals and consequent features, functional capabilities, and initial performance of the DOM MB, and
81 the operation of a combined array of DOMs as a system, are described here. Experience with the first InIce
82 strings and the IceTop stations indicates that the system design and performance goals have been achieved.

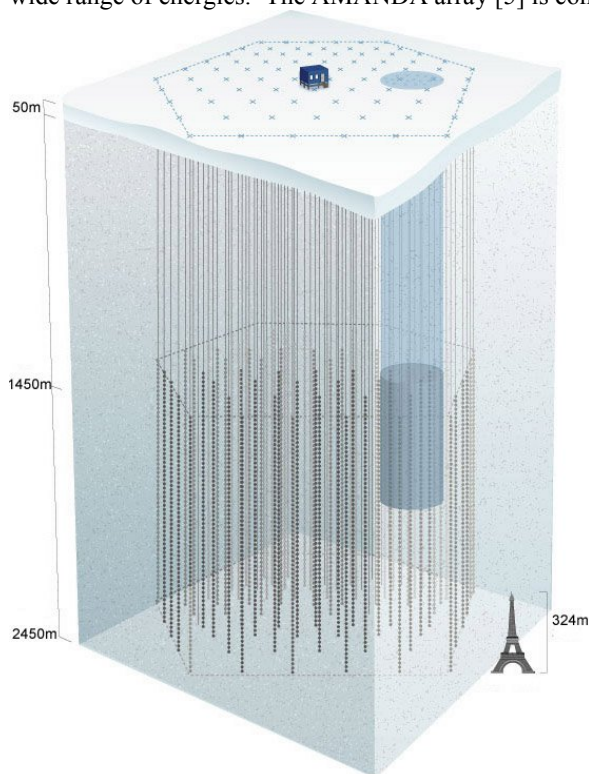
84 *PACS*: 95.55.Vj; 95.85.Ry, 29.40.Ka, 29.40.Gx

85 *Keywords*: Neutrino Telescope, IceCube, signal digitization. AMANDA

86 1. IceCube Overview

87 IceCube [1],[2] is a kilometer-scale high-energy neutrino observatory now under construction at the Amundsen-
 88 Scott South Pole station. Its main scientific goal is to map the high-energy neutrino sky, which is expected to include
 89 both a diffuse neutrino flux and point sources [3]. The size of IceCube is set by a sensitivity requirement inferred
 90 from the spectrum of Ultra High Energy (UHE) cosmic rays [4]. IceCube is designed to observe and study neutrinos
 91 with energies from as low as 100 GeV to perhaps well into the EeV range with useful sensitivity. It can also measure
 92 supernova bursts.

93 Figure 1 is a schematic representation of IceCube. A deep “InIce” array and a surface array “IceTop” are the main
 94 components of IceCube. The combination of InIce and IceTop enables the study of cosmic ray composition over a
 95 wide range of energies. The AMANDA array [5] is contained within IceCube, as shown in the figure.



96
 97 Figure 1. A perspective view of a fully instrumented IceCube detector. The 80 strings for InIce are shown. Each dot represents a DOM. The
 98 darker shaded area shows the location of AMANDA, the precursor detector. The IceCube Laboratory is also shown on the surface of the ice.

99 The detector uses the ~2800 m-thick polar ice sheet to provide a target, an optically clear radiator, and a stable
 100 instrument deployment platform. InIce consists of an array of optical sensors called Digital Optical Modules
 101 (DOMs), organized in a lattice of ultimately 80 vertical “strings”, frozen into the polar ice sheet. Each string includes

102 60 DOMs, spaced uniformly from a depth of 1450 to 2450 m. There are plans to create a densely instrumented deep
103 core in the center of IceCube by adding six special strings with more closely spaced optical modules concentrated in
104 the clearest ice toward the bottom [6].

105 A string is deployed into a water-filled hole, which has been bored with a hot-water jet. Once the water refreezes,
106 the DOMs become permanently inaccessible. Heat flow from within the earth introduces a vertical thermal gradient
107 in the ice, leading to a variation in the internal operating temperature of the DOMs from -9°C at the lowest elevation
108 DOM to -32°C at the uppermost DOM.

109 The IceTop surface air shower array consists of pairs of tanks placed about 25 meters from the top of each down-
110 hole cable and separated from each other by 10 meters. Each tank is instrumented with two DOMs frozen into the
111 top of the ice in the tanks. The DOMs capture Cherenkov light generated by charged particles passing through the
112 tanks. Typical signals are much bigger than signals in the deep ice. For example, a single muon typically generates a
113 signal with a total charge equivalent to 130 photoelectrons, and a large air shower often produces a signal equivalent
114 to tens or hundreds of muons. Operating temperatures for IceTop stations vary seasonally from -40°C to -20°C . The
115 ice temperature is about 10°C lower than the board temperature.

116 A DOM contains a photomultiplier tube (PMT), which detects the blue and near-UV Cherenkov light produced by
117 relativistic charged particles passing through the ice. Photons travel long distances due to the large absorption length
118 of well above 100 m on average. Scattering in the ice disperses photon arrival times and directions for distances that
119 are large compared to the effective scattering length of ~ 24 m. The signal shape depends on both the distance from
120 the source and its linear extent. The width in time generally increases with the track's distance from the DOM. In
121 addition, the reconstruction of InIce cascades and IceTop air showers places further requirements on the DAQ
122 architecture. The very wide range of possible energy depositions leads to a demanding requirement on dynamic
123 range in the detectors. Digital information from the ensemble of DOMs allows reconstruction of event topology and
124 energy, from which the nature of the event may be determined.

125 In this paper, we concentrate on system aspects of hardware and software elements of IceCube that capture and
126 process the primary signal information. We discuss hardware design and implementation, and demonstrate
127 functionality. The clock distribution scheme used by IceCube is novel, and so we early on focused on our ability to
128 do time calibration. Results from that effort are included. Our ability to calibrate the trigger efficiency and the
129 waveform digitizers for charge and feature extraction will be presented in a later paper.

130 Sections 2-4 provide conceptual overviews, performance goals, and basic technical aspects. Section 5 describes
131 manufacturing and testing procedures, while Section 6 summarizes the performance and reliability up to August
132 2008.

133 2. DAQ - Technical Design

134 In the broadest sense, the primary goal for the IceCube DAQ is to capture and timestamp with high accuracy, the
135 complex, widely varying optical signals over the maximum dynamic range provided by the PMT. To meet this goal,
136 the IceCube DAQ architecture is decentralized. The digitization is done individually inside each DOM, and then
137 collected in the counting house in the IceCube Laboratory (ICL), which is located on the surface of the ice.

138 Operationally, the DOMs in IceCube resemble an ensemble of satellites, with interconnects and communication
139 via copper wire-pairs. The data collection process is centrally managed over this digital communications and time
140 signal distribution network. Power is also distributed over this network. This decentralized approach places complex

141 electronic subsystems beyond any possibility of access for maintenance. Hence, reliability and programmability
142 considerations were drivers in the engineering process.

143 The goal of this architecture is to obtain very high information quality with minimal on-site personnel needed at
144 the South Pole during both detector commissioning and operation. The IceCube DAQ design relies upon the
145 collaboration's understanding of how to build a digital system after studying from the behavior of 41 prototype DOMs
146 [8] deployed in AMANDA.

147 2.1. The "Hit" – The Fundamental IceCube Datum

148 The primary function of the DOM is to produce a digital output record, called a "Hit" whenever one or more
149 photons are detected. The basic elements of a Hit are a timestamp generated locally within the DOM and waveform
150 information. A Hit can range in size from a minimum of 12 bytes to several hundred bytes depending on the
151 waveform's complexity and trigger conditions. A Hit always contains at least a timestamp, a coarse measure of
152 charge, and several bits defining Hit origin.

153 Waveform information is collected for a programmable interval – presently chosen to be 6.4 μ s, which is more
154 than the maximum time interval over which the most energetic events are expected to contribute detectable light to
155 any one DOM.

156 Hardware trigger signals exchanged between neighboring channels may be utilized by the DOM trigger logic to
157 limit data flow by either minimizing the level of waveform detail within a Hit, or by rejecting Hits that are isolated –
158 *i.e.*, with no nearby Hits in time or space, and hence much more likely to be PMT noise than real physics events.

159 2.2. DAQ Elements Involved in Generating Hits

160 The real-time IceCube DAQ includes those functional blocks of IceCube that contribute to time-calibrated Hits:

- 161 1. The *Digital Optical Module*, deployed in both InIce and IceTop.
- 162 2. The *DOMHub*, located in the ICL, and based on an industrial PC.
- 163 3. The *Cable Network*, which connects DOMs to the DOMHub and adjacent DOMs to each other.
- 164 4. The *Master Clock*, which distributes time calibration (RAPcal) signals derived from a GPS receiver to the
165 DOMHubs.
- 166 5. The *Stringhub*, a software element that, among other tasks, maps Hits from DOM clock units to the clock
167 domain of the ICL and time-orders the Hit stream for an entire string.

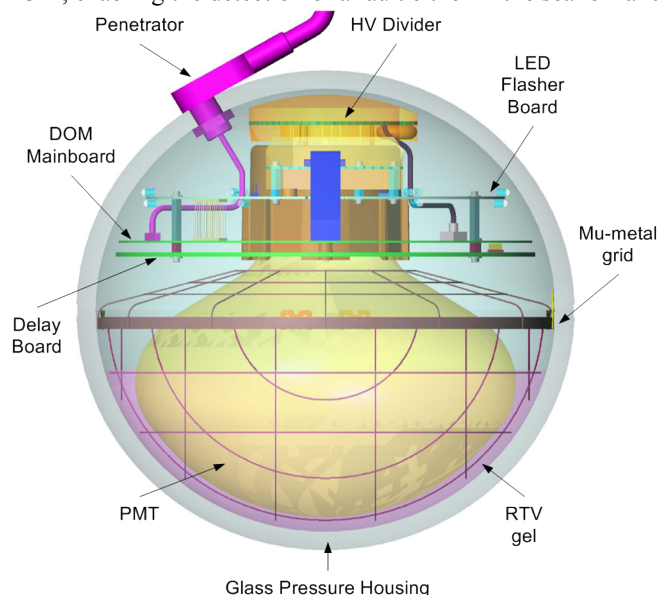
168 Together, these elements capture the PMT anode pulses above a configurable threshold with a minimum set value
169 of ~ 0.25 single photoelectron (SPE) pulse height, and transform the information to an ensemble of timestamped,
170 time-calibrated, and time-ordered digital data blocks.

171 2.3. The Digital Optical Module – Overview

172 The DOM's main elements are a 25 cm diameter PMT (Hamamatsu R7081-02), a modular 2 KV high voltage
173 (HV) power supply for the PMT, a separate passive base for PMT operation, the DOM Main Board (MB), a stripline
174 signal delay board, and a 13 mm thick glass sphere to withstand the pressure of its deep deployment. A flexible gel
175 provides support and optical coupling from the glass sphere to the PMT's face. Figure 2 is an illustration of a DOM
176 with its components.

177 The assembled DOM is filled with dry nitrogen to a pressure of approximately $\frac{1}{2}$ atmosphere. This maintains a
178 strong compressive force on the sphere, assuring mechanical integrity of the circumferential seal during handling,

179 storage, and deployment. The DOM provides built-in electronic sensing of the gas pressure within the assembled
 180 DOM, enabling the detection of a fault either in the seal or failure of the PMT vacuum.



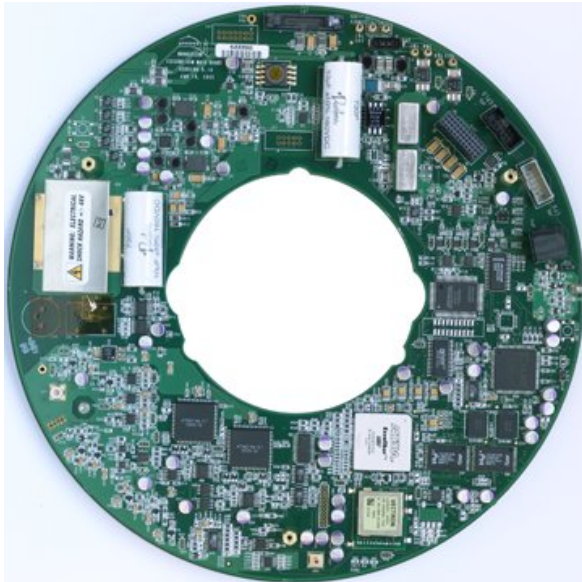
181

182 Figure 2. A schematic illustration of a DOM. The DOM contains a HV generator with divides the voltage to the photomultiplier. The DOM
 183 Mainboard or DOM MB digitizes the signals from the phototube, activates the LEDs on the LED flasher board, and communicates with the surface.
 184 A mu-metal grid shields the phototube against the Earth's magnetic field. The phototube is optically coupled to the exterior Glass Pressure
 185 Housing by RTV gel. The penetrator provides a path where the wires from the surface can pass through the Glass Pressure shield.

186 The PMT is operated with the photocathode grounded. The anode signal formation hence occurs at positive HV.
 187 This analog signal is presented to the DOM MB signal path, DC-coupled from the input to a digitizer. At the input,
 188 the signal is split to a high-bandwidth PMT discriminator path and to a 75 ns high quality delay line, which provides
 189 enough time for the downstream electronics to receive a trigger from the discriminator.

190 The DOM MB (Figure 3), the "central processor" of the DOM, receives the PMT signals. After digitization, the
 191 DOM MB formats the data to create a Hit. High-bandwidth waveform capture is accomplished by an application
 192 specific integrated circuit (ASIC), the Analog Transient Waveform Digitizer (ATWD) [9]. Data is buffered until the
 193 DOM MB receives a request to transfer data to the ICL.

194 In addition to the signal capture/digitization scheme, the use of free-running high-stability oscillators in the DOMs
 195 is an innovation that permits the precise time calibration of data without actual synchronization, and at the same time
 196 creates negligible impact on network bandwidth. Timestamping of data is realized by a Reciprocal Active Pulsing
 197 (RAPcal) [10] procedure, which is described in Section 4.7.

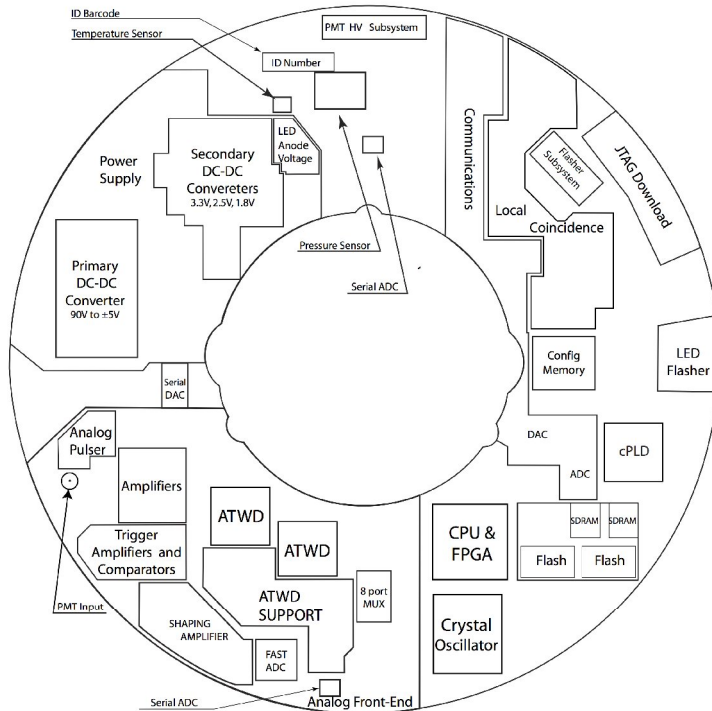


198
199 Figure 3. A photograph of the DOM MB. The diameter of the circuit board is 274 mm. This circular circuit board communicates with the surface
200 and provides power and drives the other electronics board inside the DOM. This photograph shows the location of the components, which are
201 described in the text.

202 The DOM includes a “flasher” board hosting 12 LEDs that can be actuated to produce bright UV optical pulses
203 detectable by other DOMs. Flasher board LEDs can be pulsed either individually or in combinations at
204 programmable output levels and pulse lengths. They are used to stimulate and calibrate distant DOMs, simulate
205 physical events, and to investigate optical properties of the ice. In addition, the DOM MB is equipped with an “on-
206 board LED”, which delivers precisely timed, but weak signals for calibration of single photoelectron pulses and PMT
207 transit times. A complete description of the DOM MB, including its other functions, can be found in the next section.

208 2.4. DOM MB Technical Design

209 The DOM MB’s primary components are identified in Figure 4, while the functional blocks are shown in Figure 5.
210 The top of Figure 5 shows that the analog signal from the PMT is split into three paths at the input to the DOM MB.
211 The top path is for the trigger. Below it is the main signal path which goes through a 75 ns delay line and is then split
212 and presented to three channels of the two ATWDs after different levels of amplification. Finally, a part of the PMT
213 signal is sent to an ADC designed for handling longer signals and a lower sampling speed than the ATWDs. These
214 signal paths, the electronics needed to digitize them and send the Hits to the surface, and some additional circuitry are
215 described in the following subsections.

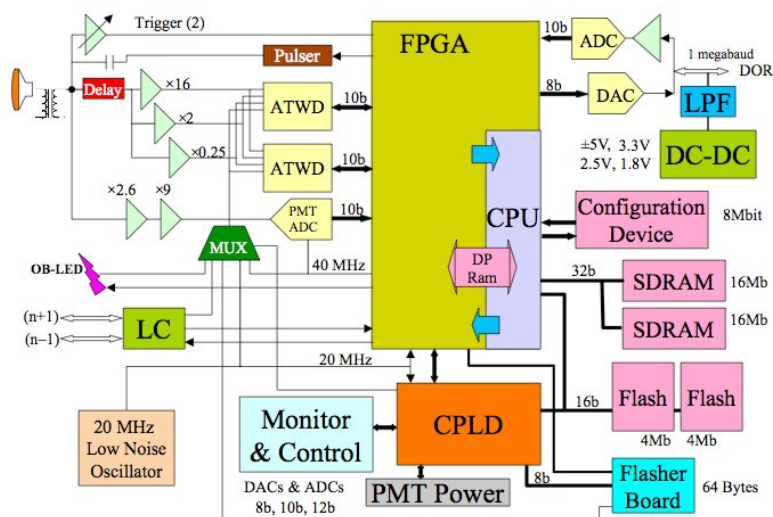


216

217 Figure 4. The location of the DOM MB functional blocks. This figure shows the subsystems on the DOM MB. It has the same orientation as
 218 Figure 3 so it is possible to locate these items on the photograph.

219 2.4.1. Power Supply

220 A single twisted pair carries communications, power, and timing signals to the DOM from the surface electronics.
 221 The pair connects to a power filter network that steers the bidirectional, differential signals to the DOM's
 222 communication interface, and provides 96 V DC power to the main DC-to-DC converter. Low equivalent series
 223 resistance ceramic capacitors and ferrite power filters at the DC-DC converter input and output effectively suppress
 224 the switching noise components up to several hundred MHz. The DC-to-DC converter provides +5 V and -5 V to
 225 circuits on the DOM main board, to a mezzanine board interface, and to a secondary DC-to-DC converter, which
 226 produces 1.8 V, 2.5 V, and 3.3 V for all on-board digital electronics. When power is applied to the DOM, the on-
 227 board power management supervisor circuit in conjunction with logic in the Complex Programmable Logic Device
 228 (CPLD) initiates the boot sequence of the DOM MB from the serial configuration memory.



229

230 Figure 5. Block diagram of the DOM MB. The triangle with an arrow in the upper left is a comparator with a variable threshold. A photon hits the
 231 photomultiplier, which is in the upper left. This signal from the photomultiplier is delayed and split to the ATWD and PMT ADC. The FPGA
 232 controls the readout. Full details of the operation of the components are described in the text.

233 Conservative engineering practices dictate that the PMT photocathode be operated at ground potential with respect
 234 to the DOM MB. With capacitive coupling, the signal droop limitation would require an impractically large value
 235 ($\sim 1 \mu\text{F}$ for a 50Ω termination). Furthermore, leakage currents in faulty/degraded high-voltage ceramic capacitors
 236 can produce noise resembling PMT pulses. An analysis of the signal and power supply loops reveals that, with
 237 transformer coupling, HV power supply noise couples much more weakly into the DOM MB input than with
 238 capacitor coupling.

239 A wide-band high-voltage pulse transformer satisfies the engineering requirements. The 30 pF of anode to front-
 240 end capacitance reduces the risk of damage to the DOM MB by discharge in the PMT base because the available
 241 energy is small.

242 The transformer exceeds the pulse rise-time requirements for short pulses ($< 8 \text{ ns}$ FWHM). Good performance
 243 depends on shunting the primary winding with a 100Ω resistor, which also provides back-termination for the DOM
 244 MB input circuit and damps ringing in the PMT anode circuit. It is important to note that long time-constants can be
 245 employed in the DOM because the average pulse rate is very low; otherwise, field build-up in the core would cause a
 246 significant baseline shift.

247 The time constants of the transformer pass the high-frequency components of the signals with negligible loss, but
 248 lead to a droop after large amplitude signals. The DOM MB digitizer pedestals are set at $\sim 10\%$ of the maximum
 249 scale, to permit the capture of waveforms with below-baseline excursions.

250 2.4.2. Analog Input Amplifiers

251 The amplifiers for the trigger subsystem tap into the decoupled PMT signal right at the DOM MB input coax
 252 connector. Also from this input, the signal is passed through a serpentine 75 ns delay line, embedded in a custom
 253 printed circuit board made with superior signal propagation materials. The delayed signal is split to three separate

254 wide-band amplifiers ($\times 16$, $\times 2$, and $\times 0.25$), which preserve the PMT analog waveform with only minor bandwidth
 255 losses. Each amplifier sends its output to separate inputs of the ATWD. The amplifiers have a 100 MHz bandwidth,
 256 which is roughly matched to the 300 MSPS ATWD sampling rate

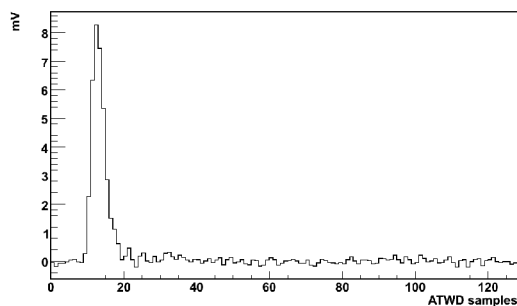
257 The circuitry confines the ATWD input signal within a 0 to 3 V range. If the input voltage were below -0.5 V,
 258 then the ATWD could be driven into latch-up; an input signal above 3.3 V would drive the ATWD into an operating
 259 condition from which it would recover slowly. Resistor-diode networks protect the inputs of the amplifiers from
 260 spikes, which might be produced by the PMT, or from static discharge.

261 2.4.3. ATWD

262 The ATWD, which is a custom designed ASIC, is the waveform digitizer for four analog inputs. Its analog
 263 memory stores 128 samples for each input until it digitized or discarded. Three amplified PMT signals provide the
 264 input to the first three ATWD channels. In addition, two 4-channel analog multiplexer chips, which can be
 265 individually selected, are the fourth input channel. The ATWD is normally quiescent, dissipating little power, and
 266 awaits a trigger signal before it converts the data to a digital signal

267 A transition of the PMT discriminator initiates the waveform capture sequence by triggering an ATWD capture.
 268 The actual ATWD launch is resynchronized to a clock edge to eliminate ambiguity in timestamps. Capture results in
 269 128 analog samples in each of the four channels. After capture is complete, digital conversion is optional, and may
 270 be initiated by the FPGA's (see Section 2.4.8) ATWD readout engine only if other logical conditions are met, as
 271 determined by the local coincidence settings and operating mode of the array (see Section 4.4). If the subsequent
 272 trigger-to-conversion conditions are not met, firmware in the FPGA resets ATWD sampling circuitry in two counts of
 273 the 40 MHz clock.

274 If trigger conditions lead to ATWD digitization, 128 Wilkinson 10-bit common-ramp analog to digital converters
 275 (ADCs) internal to the ATWD digitize the analog signals stored on a selected set of 128 sampling capacitors. The
 276 digital data are stored in a 128-word deep internal shift register.



277
 278 Figure 6. A typical single photoelectron waveform. This graph shows the measurement by the ATWD of a photoelectron produced by a photon in
 279 the ice. A few samples are digitized before the signal and many afterwards. These samples can be used to determine the normal operating
 280 baseline.

281 After conversion, another part of the readout engine transfers the data into the FPGA. The ATWD channel driven
 282 by the $\times 16$ amplifier is converted first. To provide good overlap between ranges for larger signals, the $\times 2$ gain
 283 channel is digitized, if any sample in the most sensitive channel exceeds 768 counts. If this next channel overflows,
 284 the $\times 0.25$ channel is digitized. Figure 6 shows a typical waveform.

285 Including the analog to digital conversion, transfer to the ATWD, and incidental overhead, the ATWD takes 29 μ s
286 to digitize a waveform after capture. These parallel signal paths have the dynamic range of a 14-bit 300 MSPS ADC
287 while consuming only \sim 150 mW of power without any high-speed clock or digital memory requirement. To
288 minimize dead time, the DOM is equipped with two ATWDs such that while one is processing input signals, the
289 other is available for signal capture.

290 *2.4.4. High-speed Monitoring With the ATWD Multiplexer*

291 The fourth ATWD channel is driven by either of two 4-channel analog multiplexers, permitting measurement from
292 eight signal sources on the DOM MB. Multiplexer channel 0 carries the 20 MHz signal from the internal clock
293 oscillator, as a sine wave. Channel 1 carries the frequency-doubled output of the internal FPGA phase-locked loop
294 (PLL). These signals allow the ATWD capture sampling rate calibration, the verification of the phase of ATWD
295 capture, and the clock phase for PMT waveform capture by the PMT ADC (see Section 2.4.5).

296 Signals from the on-board and the off-board LED flasher switch circuits, multiplexer channels 2 and 3, make
297 possible the measurement of PMT transit time, and the timestamping of flasher signals targeted at neighboring DOMs
298 in the array.

299 Signals from the local coincidence transceivers (see Section 4.4) appear on channels 4 and 5. These signals
300 provide diagnostic waveforms for assessing possible fault conditions with the local coincidence subsystem.

301 The communications transceiver signal on channel 6 allows calibration of the Hit timestamp with respect to the
302 precisely timed RAPcal calibration pulses transmitted to the DOM from the ICL.

303 Channel 7 monitors the output of an arbitrary waveform generator, driven by FPGA code.

304 Bits written to registers in the DOM MB CPLD separately enable each multiplexer, and select the appropriate
305 channel to be digitized. To save power, the multiplexers are shut down when not in use.

306 *2.4.5. PMT ADC*

307 Some physics signals last longer than can be captured by the ATWD. To obtain this information, there is a fourth
308 PMT signal path. This path consists of a three-stage waveform-shaping amplifier with a 180 ns shaping time. This
309 path drives a low power, high-speed, 10-bit wide, parallel output, and pipelined “PMT ADC”. The PMT ADC
310 continuously samples the bandwidth-limited PMT output signal at 40 MSPS.

311 DOM MB electronics downstream can record an arbitrarily long PMT ADC record in response to a trigger, but the
312 length of the raw PMT ADC record is chosen to be 6.4 μ s. The DOM MB is capable of triggering two clock cycles
313 after digitizing a previous event.

314 An SPE signal from the PMT produces approximately a 13-count value above the ADC’s baseline, sufficient to
315 detect its presence. This relatively low gain allows the PMT ADC to offer reasonable dynamic range.

316 *2.4.6. PMT Trigger Discriminator*

317 The DOM MB can trigger on signals from the PMT. To do this, it uses a signal from the PMT, which drives the
318 amplifier stages preceding two low power, high-speed comparators (discriminators). Each comparator has a different
319 sensitivity. The high-resolution comparator, with a nominal 0.0024 PE/DAC count, has a narrow operating range,
320 and is intended to sense SPE pulses. The low-resolution “multi-PE” comparator has a resolution that is coarser by a
321 factor of 10 and therefore has a wider operating range.

322 At the nominal InIce PMT gain of 1×10^7 , the low system noise and low device noise allow the PMT trigger level
323 to be set as low as 1/6 SPE. At this threshold, there is no significant increase in trigger rate due to electronic noise.

324 Also, these two comparators enable the implementation of multi-level event recognition. For example, the IceTop
325 high gain DOMs (5×10^6) utilize the multi-PE discriminator for triggering, with its threshold set to an amplitude
326 corresponding to a pulse of 10 PEs. In addition, these two comparators are used in self-local coincidence mode,
327 which is described in Section 4.4.3.

328 *2.4.7. Local Coincidence Trigger Circuit*

329 When a trigger comparator fires, two state machines are activated to send local-coincidence digital signals to
330 adjacent DOMs (above and below) through bidirectional, fully duplex transceivers connected to a dedicated network
331 of twisted wire pairs.

332 Local coincidence receivers on each DOM deliver signals into the trigger system of the FPGA and into a relaying
333 state machine. This local coincidence relaying engine, if enabled, forwards a message beyond the nearest neighbor
334 DOM. The scheme makes possible coincidence between nearest neighbors, next-nearest neighbors, and so on. If a
335 DOM originates and transmits a local coincidence (LC) signal, it will not relay the redundant LC signals from its
336 neighbors.

337 *2.4.8. FPGA and ARM CPU*

338 The Altera EPXA-4 FPGA handles signal and communications processing. The CPU handles data transport,
339 system testing and monitoring. The CPU initiates FPGA reconfiguration, in real-time, as dictated by the
340 requirements of data acquisition and system testing. This highly integrated system on a programmable chip (SOPC)
341 architecture confines high speed, high data bandwidth signals to a single die on the DOM MB, which reduces noise
342 and saves power.

343 The Hit processing portion of the FPGA contains trigger logic, an ATWD readout engine for each ATWD, a Hit
344 record building engine, a data compression engine, and a direct memory access (DMA) controller. A DMA engine
345 transfers Hit records into main memory for subsequent transmission to the ICL. It also implements on-board and off-
346 board flasher control logic, PMT ADC data handling, communications protocol state machines, communications
347 ADC, and DAC data handling.

348 The communications processing portion of the FPGA contains a half-duplex signaling protocol engine and
349 modulation and demodulation function blocks, which drive a communications digital to analog converter (DAC) and
350 monitor a communications ADC respectively.

351 The Altera chip also provides IceCube with a supernova (SN) search capability. A SN event, if yielding a
352 sufficiently intense flux of MeV neutrinos at earth, will cause a global increase in the ambient light deep in the ice. A
353 rate increase, seen by all DOMs, provides an unambiguous signal for such an event. The chip records the rate of Hits
354 - binning Hit times at the few ms level.

355 *2.4.9. Memory (SDRAM, Flash, Flash Files)*

356 The EPXA-4 architecture supports SDRAM (synchronous dynamic random access memory) for main memory, an
357 SRAM (static random access memory) interface for low-performance memory, memory-mapped peripherals, and
358 flash memory. The DOM MB includes two 16 MB SDRAM memory chips, two 4 MB flash (non-volatile)
359 memories, and a 4 Mb configuration memory.

360 When the DOM is powered up, the serial configuration memory uploads a configuration into the EPXA4's FPGA
361 and program code into the EPXA4's CPU's memory. The configuration memory can only be programmed before the
362 DOM is sealed and cannot be reprogrammed after deployment. Its contents include a base-band communications
363 package for the FPGA, a utility program for the CPU so that the flash memory chips are loaded, and a command

364 interpreter for rebooting to the boot-block in either flash memory. This is analogous to a desktop computer booting
365 to block 0 of its hard disk.

366 The two 4 MB boot-block flash memories are organized as a log structured flash memory file system. The file
367 system stores CPU programs, FPGA configuration files, and interpreter scripts. Various files support production
368 testing, integration after deployment, and Hit data acquisition. Any and all files may be updated after the DOM is
369 deployed into the ice. Each flash memory also contains a 64-bit serial number, from which we derive a unique 48-bit
370 DOM ID. The DOM ID maps to the geometrical position of each DOM. Furthermore, unique DOM parameters can
371 be loaded by DAQ control from a database indexed by the DOM ID.

372 After reboot, the CPU executes program code copied into SDRAM. Approximately half of the SDRAM is
373 allocated as a circular buffer for DMA Hit record transfers from the FPGA. The CPU accesses registers in the CPLD
374 and Flasher Board interface through the Expansion Bus Interface (EBI). Flash memory also resides on the EBI.

375 *2.4.10. DOM Local Oscillator*

376 The DOM's 20 MHz temperature-compensated crystal oscillator has a certified stability of roughly 1×10^{-11} for a
377 sample interval of 5 seconds.⁸ In practice, the crystal frequency and phase drifts become significant typically only
378 after several minutes. The 20 MHz oscillator output drives the clock inputs of the FPGA, the communications ADC,
379 the communications DAC, and the reference clock signal port of the flasher board interface. A phase locked loop
380 (PLL) in the FPGA doubles the frequency to 40 MHz. This 40 MHz signal drives a 48-bit local clock within the
381 FPGA, the DOM local clock; it rolls over every 81.4 days. The DOM local clock is used to timestamp Hits recorded
382 by the DOM and the RAPcal timing calibration packets exchanged between the DOM and the DOMHub. The 40
383 MHz reference also drives the clock input of the PMT ADC.

384 *2.4.11. Communication With Surface*

385 As communication and power must share the same wire pair, it is necessary to separate them at the DOM MB.
386 Balanced L sections at the power filter input confine the communications signals to the communications front-end
387 receiver. A Π section filters the power and isolates the DOM communications interface from switching noise.

388 Ceramic capacitors couple communications signals between the twisted pair and the communications transformer.
389 The grounded center tap of the transformer accommodates the topology required by the 8-bit current-mode
390 communications DAC clocked at 20 MHz. The choice of current mode DAC allows two DOMs to share the InIce
391 end of the main cable pair. The end-most DOM on the pair must be terminated in the characteristic impedance of the
392 twisted pair. The unterminated DOM typically bridges onto the twisted pair 17 meters upstream from the terminated
393 DOM; the additional stub introduces a small, systematic time error. The modulator produces differential signals with
394 amplitudes of approximately 2 V (depending on communications parameter settings) onto the twisted pair.

395 The center-tapped secondary of the transformer also drives a $\times 5$ differential amplifier stage characterized by high
396 common mode rejection ratio (CMRR). The high CMRR reduces the susceptibility of the DOM line receiver to
397 interfering signals such as electromagnetic interference (EMI) or radio frequency interference (RFI). The amplifier
398 drives a 10-bit, 2 V input-span, ADC that samples the communications waveform at 20 MSPS. The parallel output
399 stream of ADC data drives the inputs of the communications receiver firmware in the FPGA.

⁸ Vectron International manufactures the model C2560A-0009 TCXO module specifically for IceCube. Since the oscillator is crucial to DOM performance, the brand and model were selected based on Allen variance performance and power consumption. The procurement specification required 100% Allen variance testing.

400 The topology resembles that of the commonly used T-1 communications links. So, the natural choice was
401 Amplitude Shift Keying⁹ (ASK) with a transmission rate of 1 Mb/s, which includes encoding bits. Since we have
402 selected ASK modulation, and multiple DOMs share wire pairs, it is necessary to utilize half-duplex. The
403 communications master resides in the communications card within the DOMHub in the ICL. That master alternately
404 sends commands to and requests data from the two DOMs sharing the InIce end of the wire pair.

405 The distribution rate of RAPcal signals from the ICL to all DOMs must accommodate any oscillators with
406 marginal short-term stability. The stability requirement for the DOM local oscillator is that RAPcal signals be
407 distributed to all DOMs in the array at least as often as every 5 seconds. However, the complete DOMHub-to-DOM-
408 to-DOMHub exchange of RAPcal signals consumes less than 1.5 ms, so the sacrifice of system communications
409 bandwidth to time calibration is negligible.

410 2.4.12. CPLD

411 The DOM depends upon certain higher-level logic functions and state machines that cannot be implemented in the
412 FPGA because the FPGA does not retain its logic configuration through power cycling. Those logic functions are
413 implemented in a CPLD.

414 The CPLD code contains a state machine that controls the booting of the EPXA4, initiated by the rising edge of
415 the *not-power-on-reset* (nPOR) signal of the power supervisor chip. The logic in the CPLD assures that all power
416 supplies are at voltage and stable, and that internal initialization of other complex components of the DOM has been
417 completed before the configuration memory uploads its contents into the EPXA4's CPU and FPGA configuration.

418 The CPLD code also contains an interface between the EBI memory bus and the high-speed interface connector
419 used by the external LED Flasher Board. The bus interface prevents possible catastrophic failure of the flasher or a
420 generic daughter card from disrupting the memory bus the CPU relies upon for booting to its normal running-mode
421 configuration which is read from flash memory.

422 The applications programmer interface (API) of the CPLD appears to the CPU as read-only and write-only
423 memory in EBI address space. Control register bits enable or disable the high voltage power interface for the PMT,
424 the voltage source for the on-board LED flasher, the Flasher Board interface, and the pressure sensor.

425 The CPLD firmware controls the reading of 24 channels of the slow (serial) ADC used for monitoring and
426 diagnostic purposes. It also sets the 16 slow (serial) DAC outputs used to control ATWD operating parameters,
427 trigger comparator levels, and ADC reference levels. A separate serial interface supports the control and read-out of
428 PMT high voltage module.

429 The CPU may control whether it reboots from the serial configuration memory (boot to Configboot), or to flash
430 memory (boot to Iceboot), by executing a CPLD function. Another CPLD function actually initiates reboot.

431 The CPU may boot from either of the two flash memory chips. The Configboot program supports a CPLD
432 function, which virtually exchanges flash-0 for flash-1, allowing the recovery from failure of the flash-0 boot block
433 subsequent to deployment.

434 Several registers contain read-write scratch-pad bits. Scratch-pad data are retained through reboot, allowing a
435 limited amount of crucial context information that can be retained through reboot.

⁹ The communications interface design is compatible with phase modulation schemes, which offer higher data rate, superior noise immunity and timing precision, as well as full duplex communications.

436 *2.4.13. On-board Electrical Pulser*

437 Many DOM calibration programs depend upon a built-in signal source that produces waveforms similar to SPE
438 PMT pulses. The pulser injects charge that is stored on a capacitor into the analog input of the DOM MB, at the
439 PMT cable connector. A serial DAC, controls the pulser amplitude up to roughly 40 PE, in 0.04 PE steps.

440 The shape design was based upon previous measurements. Care was taken to minimize noise into the DOM MB
441 when the pulser was activated. Recent results show that the pulser shape is slightly wider than an actual PMT shape.

442 *2.4.14. On-board LED pulser*

443 Each DOM MB includes a pulse forming circuit driving an ultraviolet LED that has a wavelength of 374 nm. The
444 function of the on-board LED pulse is to stimulate the local PMT, whereas the function of the Flasher Board is to
445 stimulate neighboring DOMs.

446 A state machine in the DOM initiates a trigger, and simultaneously sends a trigger pulse to the LED flasher circuit.
447 The flasher circuit dumps a current pulse into the LED via a "shunt" which produces a voltage pulse across it. The
448 pulse propagates from the pulser circuit to the MUX connected to ATWD channel number 4. The LED flash
449 produces light, which bounces over to the PMT. The ATWD simultaneously captures PMT input and the current
450 shunt input. The time difference between the current pulse and the PMT pulse is the transit time of the PMT, delay
451 line, other circuit components.

452 The LED flash brightness can be adjusted to produce zero to a few tens of photoelectrons at the photocathode of
453 the PMT. The brightness range of the on-board LED is sufficient to measure the transit time over several orders of
454 magnitude of PMT gain around the typical operating point. Controlled weak flashes (optimally around 1%
455 occupancy) makes possible the assessment of the SPE behavior of the PMT.

456 *2.4.15. Interface to PMT Power Supply Daughter-card*

457 The DOM MB controls and powers the PMT HV subsystem, which resides on a mezzanine card atop the Flasher
458 Board. The control signals, the serial bus signals, system ground, and raw power are delivered to the HV module
459 through a ribbon cable.

460 The CPLD of the DOM MB contains a control register with one bit allocated to enable the high voltage control
461 board, and another bit allocated to enable the high voltage output of the high voltage module on the HV control
462 board. The HV control board contains two synchronous serial (SPI protocol) devices, a serial DAC for high voltage
463 control, and a serial ADC for monitoring the HV module output voltage.

464 The serial bus clock, control, and data lines of the HV subsystem interface use CPLD pins and firmware that is
465 independent of the on-board monitoring serial bus, which is also supported by the CPLD and firmware. This feature
466 prevents a failure causing disruption of the on-board serial bus from interfering with the operation of the high voltage
467 subsystem, and vice-versa. The CPLD firmware also contains code to read the serial number chip built into the HV
468 interface card.

469 *2.4.16. Interface to the Flasher Board; a Generalized High-speed Interface*

470 The DOM MB includes a 48 pin, high-speed, memory mapped interface to the Flasher Board. The connector
471 delivers power, an extension of the EBI memory bus, and control lines from the DOM MB FPGA to the daughter
472 card. The connector also delivers system clock and trigger control signals directly from the FPGAs.

473 This interface delivers a power-enable line to the daughter card. When this line goes high, the daughter- card is
474 permitted to draw power and connect to the memory bus interface. Likewise, an enable is transferred to the bus

475 extension enable firmware in the CPLD. This feature allows a 30% saving of power, since the calibration capability
476 provided by the high intensity flashers is rarely needed.

477 When the power-enable line goes low, the daughter card powers off all electronics, and disconnects from the bus
478 extension. If the DOM power supervisor should detect an event that causes nPOR to be asserted, then the power-
479 enable line is set to the default (low state) and the memory bus repeater built into the CPLD breaks connection with
480 the EBI memory bus. This buffering feature protects the primary data-taking capability of the DOM MB from being
481 compromised should there be a catastrophic failure of the flasher card.

482 The interface has 8 bidirectional data lines, a read line, a write line, and 6 address lines to the daughter card. This
483 is sufficient to control a wide variety of states in the daughter card, as well as permitting the transfer of arbitrarily
484 large data sets in either direction. The data requirements of the Flasher Board are, however, modest.

485 Control lines from the FPGA of the DOM MB notify the Flasher Board when to initiate a flash. The Flasher
486 Board produces an output pulse whose voltage is proportional to the flash amplitude. That signal is sent through a
487 coax cable to a multiplexer input of the ATWD for timing calibration purposes.

488 The interface includes a low-voltage differential signal (LVDS) 20 MHz clock pair derived from the DOM MB
489 system clock. This feature is useful for synchronizing it with the DOM MB activity. It also contains a set of control
490 and I/O lines configured as a JTAG¹⁰ programming interface. The interface allows firmware to be updated in the
491 flasher board after the DOM has been deployed in the ice.

492 *2.4.17. Monitoring with the Slow ADCs*

493 Two serial ADCs (I2C protocol) monitor a total of 24 voltages in the DOM. The ADC readouts are particularly
494 useful in the test stage of newly manufactured DOM MBs. They also provide some diagnostic information should
495 the DOM suffer a partial failure after deployment.

496 Channels 0, 1, 9, 10, and 11 monitor power supply voltages. Channel 2 monitors the (DOM) pressure sensor on
497 the DOM MB. The voltage measurement on Channel 0 is necessary to calibrate the pressure measurement.

498 Channels 3, 4, 5, 6, and 7 monitor the current delivered by all major power supplies on the DOM MB. Channels 8
499 and 12 monitor control voltages of the front-end discriminator thresholds. Channel 13 monitors the reference voltage
500 of the high speed ADC. Channel 14 monitors the voltage delivered to the on-board LED pulser. Channels 15-22
501 monitor control voltages produced by serial DACs, which control ATWD behavior. Finally, channel 23 monitors the
502 voltage of the front-end test-pulse control.

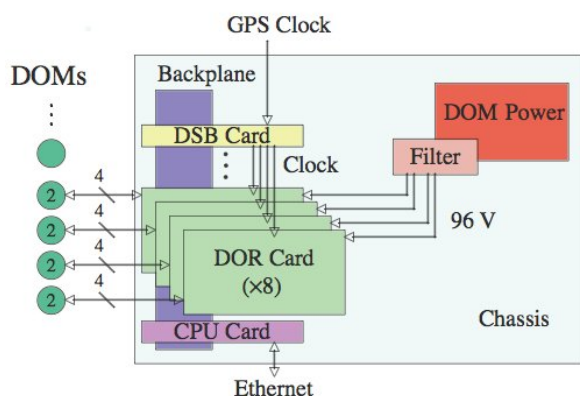
503 *2.5. The Cable Network*

504 The cable network carries power and signals between the DOMs and the DOMHub. The cable is of sufficient
505 quality that the amplitude-shift modulation scheme reliably yields data rates up to ~900 kb/s for the most remote
506 DOMs in the array. By sharing two DOMs on one pair, only one cable is needed for a string, substantially reducing
507 costs. This cable size, roughly 3 cm in diameter, approaches the practical limits for transportation volume and weight,
508 flexibility, and strength during deployment.

509 The down-hole cable consists of 20 quads. Fifteen quads are used for signals to the DOMS while one is for LC.
510 Each quad contains two pairs of wires. The DOM Quad services four DOMs. Three twisted pairs from the cable
511 enter the DOM in the location identified as the Cable Penetrator Assembly seen in Figure 2. Two of these pairs are
512 the LC links to adjacent DOMs; the third pair connects the DOM to the DOMHub.

¹⁰ Joint Test Action Group IEEE Standard 1149.1-1990.

513 A surface cable from ICL connects to a surface junction box located near the top of each hole. The surface cable
 514 contains extra wire quads in an inner, shielded core to service the two IceTop tanks associated with each hole. Data
 515 rates for IceTop DOMs are higher than for InIce DOMs, so only one IceTop DOM is connected to its corresponding
 516 DOR card input. However, to maintain commonality throughout IceCube, the control and communications protocol
 517 and baud rate are the same as for cable pairs. IceTop DOMs also exploit an LC communication link between the two
 518 tanks at each station.



519
 520 Figure 7. A block diagram of the DOMHub. The left hand side depicts the data from a string of DOMs. The label 2 in the left circles refers to the
 521 fact that two DOMs are on each wire pair. The number 4 refers to the fact that each DOR card digitizes four DOM pairs. The DOM Hub contains
 522 a power supply, a CPU Card and the DSB card for timing. The DOR cards communicate over the backplane. A DOMHub communicates with the
 523 trigger and event builder over Ethernet.

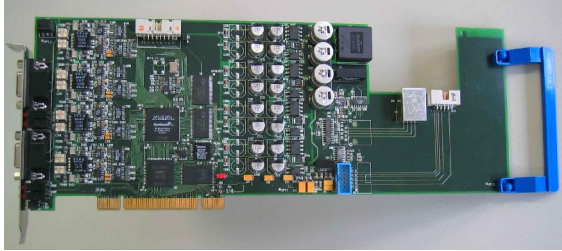
524 2.6. The DOMHub

525 The DOMHub is a computer in the ICL that communicates with all of a string's DOM MBs. Its block diagram
 526 can be seen in Figure 7. Its components are housed in a standard 24" deep industrial PC chassis. The PCI bus
 527 backplane accommodates 8 DOR cards, one DOMHub Service Board (DSB), and one low power single board
 528 computer (SBC).

529 Each DOR card can communicate with eight DOMs, so the DOMHub can host 64 DOMs. In practice, a
 530 DOMHub hosts an entire string of 60 DOMs for InIce, or 32 DOMs for IceTop (8 stations).

531 2.6.1. The DOM Readout (DOR) Card

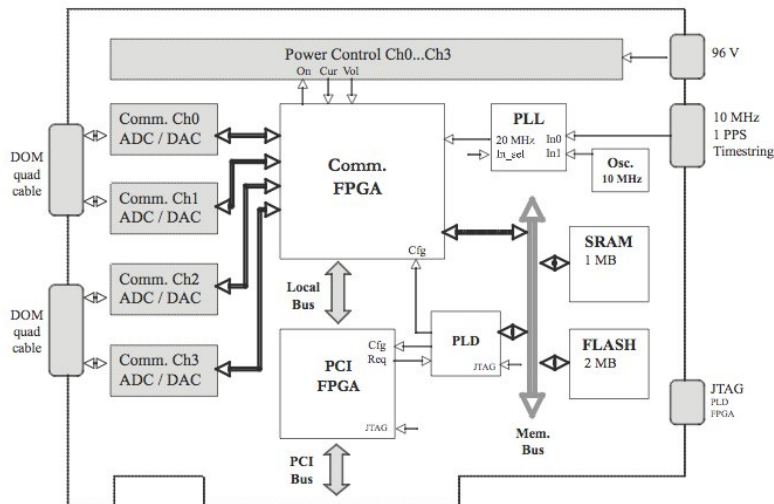
532 The DOR card is a full-size full-custom PCI card, shown in Figure 8. Each DOR card handles communications
 533 with the DOMs connected to its four wire-pair inputs and the DOR Driver, the lowest level software element of the
 534 DAQ chain in the ICL. The block diagram in Figure 9 shows the media access interfaces, and power control
 535 functions of the DOR card.



536
537 Figure 8. A photograph of a fully functional DOR card.

538 The DOR card controls power to the DOMs, establishes that boot-up has occurred properly, selects which code the
539 DOM is to run (or downloads new code), establishes a conversation that may include calibration tasks or block data
540 transfer, senses fault conditions, manages time calibration sequences, controls the DOM state, or initiates any of the
541 numerous and diverse DOM actions.

542 A utility function loads the FPGA configuration files into flash memory. Other functions cause the
543 communications FPGA to be reloaded from flash memory, select the clock source, initiate RAPcal, signal exchanges
544 with DOMs, and other features described in the next section.



545
546 Figure 9. This figure shows the functional blocks of a DOR Card. On the left shows the signals from the DOMs. The COM ADC/DAQ digitizes
547 the signals from the DOMs and sends signals to the DOM over the wire pairs on the quad cable. The Communication FPGA drives these ADCs.
548 Memory is shown as well as the exterior communications and power to the DOR card.

549 2.6.2. PCI Block

550 The firmware of the PCI bus interface FPGA includes a commercial VHDL PCI core adapted to suit the
551 requirements of the DOR card hardware and DOR driver. The 32-bit core supports master/slave control logic, and 33
552 MHz bus speed. The PCI core is compliant with “PCI Local Bus Specification revision 2.2”.

553 The PCI FPGA executes bi-directional programmed (single bus cycle) 32-bit transfer to thirty-two control and
554 status registers. The firmware also contains code for 32-bit quad-word aligned DMA (Direct memory access) writes
555 of data to main memory on the CPU board in the PC chassis.

556 2.6.3. DOM Power Management

557 The DOR driver can cause the ± 48 V power for any of the 4 wire pairs to be switched on or off. Both wires of a
558 pair are switched for symmetry and safety. Also, for safety, power is applied only when a cable connection is sensed.
559 The switches have built-in slew-rate limiting to reduce component stresses, and suppress power on/off transient
560 noise.

561 The DOR card has ADC's for monitoring wire pair current and voltage. A "proc file" interface of the DOR driver
562 allows the voltage and current values to be read by user programs, or from the command line. Furthermore, a
563 firmware component detects pair over- current or under-current conditions and then removes power to the pair.

564 2.6.4. DSB Card

565 The DSB card is a very simple electronics board. Its primary function is to distribute the system timing and
566 reference signals to each of the eight DOR cards in a DOMHub. The inputs to this board include the 10 MHz system
567 clock, 1 Hz, and Global Position System (GPS) reference signal (see Section 2.7). These signals originate in a GPS
568 receiver in the ICL and are distributed isochronously to all DOMHubs.

569 2.6.5. Time Calibration

570 The DOR card receives the clock signals from the DSB Board. A PLL on the DOR card produces the 20 MHz
571 global clock, which drives the 56-bit clock counter in the communication FPGA of each DOR card. The 1 Hz signal
572 triggers a snapshot of the 56-bit counter value every second. The DOR clock counter rolls over every 114.24 years,
573 and is never explicitly reset. The counter snapshots together with the corresponding encoded time of day provide a
574 cross reference between the DOR card's local clock value and the UTC time.

575 Software may initiate a time calibration. The DOR firmware completely manages the time calibration process.
576 The cycle produces a RAPcal data packet containing DOR and DOM timestamps and digitized RAPcal received
577 pulse waveforms.

578 2.6.6. DOR card Flash Memory and FPGA Configuration

579 The communications controller FPGA configuration image resides in page 0, 1, or 2 of a 2 MB Flash memory.
580 The PCI bus interface FPGA image resides in page 3. Loading the communications image into flash depends on the
581 integrity of the PCI image. Consequently, the PCI image is protected.

582 The two FPGAs and the CPLD share a JTAG chain. At time of DOR card manufacture, first, the CPLD must be
583 programmed via JTAG, and then the PCI FPGA must be loaded via the JTAG. Power must be kept on until flash is
584 loaded. UNIX utility programs write configuration files to flash memory pages through the DOR Driver's Linux file
585 system proc file interface. Validity checking in the DOR Driver prevents invalid images from being loaded into
586 DOR card flash. The JTAG chain provides a means for loading test firmware into either FPGA.

587 Once flash is loaded, the application of power, or a PCI bus reset, causes a CPLD on the DOR card to read
588 configuration data from flash memory, serialize it, and transfers it to an in-circuit programming interfaces of each
589 FPGA. The communications FPGA may be reloaded at any time by issuing a command to the DOR Driver; the PCI
590 FPGA may be reloaded on the fly, but this is risky in case the new image contains a bug.

591 Each DOR card, after final assembly and test, has a unique ID, as well as a final test summary, written into the
592 uppermost 64 K byte sector of the flash memory. The code contains the card revision number, the production run
593 number, and the card serial number, which matches the card's label. The production information may be read from
594 the DOR driver proc file interface.

595 2.7. The Master Clock and Array Timing

596 The two central components of the IceCube timing system are the Master Clock, providing each DOMHub with a
597 high precision internal "clock" synchronized to UTC [11] and the calibration process RAPcal described in Section
598 4.7. Together, these manage the time calibration as a "background" process, identically for InIce and IceTop.

599 The Master Clock makes use of the Global Positioning System (GPS) satellite radio-navigation system, which
600 disseminates precision time from the UTC master clock at the US Naval Observatory to our GPS receiver in the ICL.
601 Algorithms in the GPS receiver clock circuit make small, but abrupt, changes to crystal oscillator operating
602 parameters according to a schedule optimized for GPS satellite tracking. The abrupt parameter changes, and phase
603 error accumulation intervals result in deviations from UTC of typically 40 ns RMS over time scales of hours, but not
604 exceeding 150 ns.

605 The GPS reference time for IceCube is the phase of the 10 MHz local oven-stabilized crystal reference oscillator
606 in the GPS receiver. This oscillator is optimized for excellent Allan variance performance. Altogether, the system
607 delivers an accuracy of about ± 10 ns averaged over 24 hours.

608 The fan-out subsystem distributes the 10 MHz, the 1 Hz (as a phase modulated 10 MHz carrier), and encoded
609 time-of-day data from the GPS receiver to DOMHubs through an active fan-out. The encoded GPS time data,
610 contains second, minute, and hour of the day, day of the year, and a time quality status character.

611 The principal engineering requirements for the fan-out are low jitter, high noise immunity, simplicity, and
612 robustness. The 10 MHz and 1 Hz modulated 10 MHz signals pass through common mode inductors at the
613 transmitter and receiver end to improve noise immunity and effectively break ground loops between apparatus widely
614 dispersed in the ICL. For the encoded time of day information, RS-485 was chosen for its noise immunity. Each
615 distribution port of the fan-out has its own line drivers to insure that any particular failure has minimal impact on
616 neighboring distribution ports.

617 The Master Clock Distribution System and interconnecting cables delay the arrival of time reference signals
618 traveling from the GPS receiver to the DOMHub. All signal paths between the GPS receiver's 10 MHz output, via
619 fan-outs to the DSB, and to each DOR card are matched within 0.7 ns RMS. Thus, the DOR cards "mirror" the
620 Master Clock with an accuracy of less than 1 ns.

621 A static offset must be applied to the experimental data to map IceCube Time (ICT) to UTC. ICT differs from
622 UTC by the master clock distribution cable delay plus the GPS to UTC offset.

623 The DSB card in each DOMHub distributes the three signals to each of the eight DOR cards. The DOR card
624 doubles the GPS frequency to 20 MHz and drives a clock counter. When the 10 MHz clock signal goes high
625 immediately after the 1 Hz GPS signal goes high, logic in the DOR card's FPGA latches the clock counter value and
626 the time of day data from the GPS receiver from the previous second to form a time sample record. This time
627 sampling engine stores its output in a 10-reading deep first-in first-out (FIFO) memory. Data acquisition software
628 running in a DOMHub's CPU reads these records from a Linux file system proc file and forwards them to a data-
629 logging computer where they become part of the physics data set.

630 In operation, the clock counter value in each DOR card increments exactly 2×10^7 counts every second. A
631 module in the DOR card firmware confirms that 2×10^7 additional counts are registered each second to verify clock
632 integrity, and firmware correctness, and freedom from injected noise.

633 3. Firmware and Software

634 In the universe of computers, the DOM resembles a hand held device since it does not have a mass storage device
635 like a disk drive. The DOM does not need “processes” in the sense of UNIX, nor “task scheduling.” However,
636 interrupt handlers are used for communications and data collection. Therefore, an open source collection of standard
637 UNIX-like single threaded functions called “newlib” [12] was chosen instead of more sophisticated embedded
638 operating systems like Windows CE, embedded LINUX, or NetBSD. Newlib functions streamline common tasks
639 such as memory allocation and string operations. Communications on the DOM side, including a custom
640 communications protocol, are largely implemented in FPGA firmware.

641 3.1. DOM Software

642 At power on, firmware embedded in the Altera EPXA4 chip (called the logic master) copies a simple, robust
643 bootstrap program named *Configboot* from a read-only serial configuration memory into internal SRAM, configures
644 the FPGA, and initiates the execution of program code at the start of SRAM. The *Configboot* program interprets a
645 very small set of terse commands that allow the DOM to reboot to the image in the boot block of the primary flash
646 memory, boot from other locations in either flash memory, or boot from a dedicated serial port. A *Configboot*
647 command allows reprogramming flash memories via the communications interface to allow the users to easily
648 upgrade a DOM with new operating software and firmware. Furthermore, if flash chip 0 were to fail, *Configboot* can
649 be configured to boot the DOM’s CPU from flash chip 1.

650 Each DOM uses a reliable, journaling flash file system spanning the pair of flash memories into which a release
651 image is loaded. The release image consists of data files, software programs for test and data acquisition, and FPGA
652 configurations that suit the requirements of the software programs. The release file is built on a server computer from
653 components of a software development archive.

654 Booting from flash block 0 causes the DOM’s CPU to copy a fully featured program, called *Iceboot*, into
655 SDRAM, and start executing it. The program *Iceboot* is built of layers: low-level bootstrap code; Newlib code; a
656 Hardware Access Layer (HAL) used to encapsulate all hardware functions provided by the CPLD; the application
657 program/server; and the FPGA, including the communications interface. The *Iceboot* program presents a Forth
658 language interpreter to the user. From the interpreter’s prompt, one can invoke HAL routines directly, write data to,
659 and read data from memory addresses, reconfigure the FPGA, and invoke other applications programs like the DOM
660 Application (*Domapp*) used for data acquisition.

661 The *Domapp* program implements a simple binary-format messaging layer on top of the DOR to DOM error-
662 correcting communications protocol. Messages are sent to particular “services” within the *Domapp* (e.g. “Slow
663 Control”, “Data Access”). Each message targets a particular function (e.g., “Slow Control - set high voltage” or
664 “Data Access - fetch latest Hit data”). Every message to the DOM generates a single response, and no DOM sends
665 data unless queried. Messages are provided for configuring the hardware and for collecting and formatting the
666 physics data from buffers in main memory. Other messages provide for buffering and retrieving of periodic

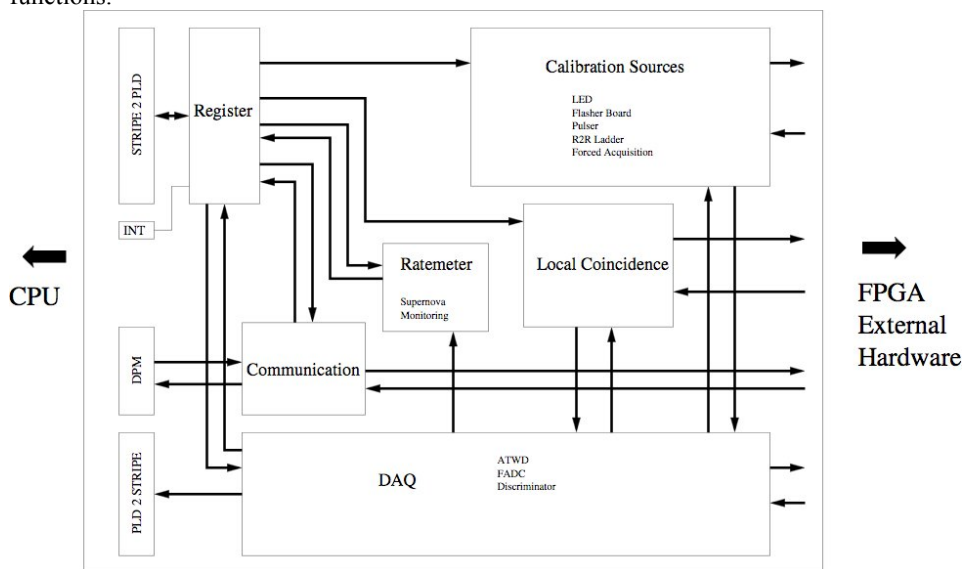
667 monitoring data describing the DOMs internal state and any exceptional conditions that may occur. The message can
 668 be logged or acted upon by the DAQ components in the ICL.

669 Typically, between runs, the DOM is rebooted into *Iceboot* to guarantee its state at the beginning of each run.
 670 Should the DOM become unresponsive, a low-level communications message sent directly to the communications
 671 firmware in the FPGA will force the DOM to reboot to *Iceboot*. Power cycling of the DOM is seldom necessary to
 672 reinitialize the DOM, and is avoided to minimize electrical stress.

673 3.2. DOM Firmware

674 The DOM Firmware suite consists of three different FPGA designs, needed for different actions. The designs are
 675 called: the *Configboot* design, the *Simple Test Framework (STF)* design, and the *Domapp* design. Only one of these
 676 can run at a given time. DOM firmware is written in VHDL supplemented with several other code generation tools.
 677 A communications firmware block is common to all three designs. Only the *Domapp* and *STF* firmware designs
 678 manipulate data acquisition hardware. The FPGA firmware design uses about two thirds of the available resources.

679 In general, the FPGA acts as an interface between the software running on the CPU and the DOM hardware.
 680 Beyond this basic logic functionality, the DOM firmware performs time-critical processing of triggering, clock
 681 counter, and PMT data (with sub-nanosecond precision); basic data block assembly; DMA of physics data to
 682 SDRAM; and communications processing. The FPGA also hosts calibration features, and Flasher Board control
 683 functions.



684
 685 Figure 10. The figure shows a functional block diagram of the firmware modules used in the main data acquisition FPGA, which is used in
 686 conjunction with Domapp. The arrows on the right indicate connections to hardware on the DOM MB. The arrows show the direction of data
 687 flow. The four boxes on the left are internal interfaces to the CPU. They include communications between the FPGA and CPU (STRIPE2PLD
 688 and PLD2STRP), dual port memory (DPM), and interrupts (INT). The other rectangles are code modules for the FPGA. These blocks describe
 689 the specific tasks. For instance, the block labeled "Ratemeter" stores information for the supernova trigger, monitoring, and dead time. The
 690 module "Register" contains the memory mapped registers for configuration and status information.

691 The *Configboot* FPGA design contains only minimal required functionality to provide communications to the
692 DOR card. Implementation of a simple, reliable, and robust design was a firm requirement because *Configboot*
693 cannot be upgraded once a DOM has been deployed into the ice.

694 The *STF* design is used primarily for DOM hardware testing. Software uses the STF program to manipulate, test
695 and verify the functionality of each hardware subsystem.

696 The *Domapp* design, shown schematically in Figure 10, provides for data acquisition. Based on the settings of bits
697 in memory mapped control registers according to applications programmer interface (API) documentation, the FPGA
698 autonomously collects waveforms from the ATWD and the PMT ADC. It processes the waveforms, builds the hit
699 record according to a hard-coded template, and transfers the data through DMA to a block of the CPU's memory.
700 Parallel to data acquisition, the firmware supplies PMT count-rate meters, which are read from data registers in the
701 API; count-rate metering facilitates the supernovae detection science goal. In addition, the firmware modules control
702 the on-board calibration sources and the Flasher Board.

703 3.3. *DOMHub* Software

704 Software on the *DOMHub* builds on the rich set of DOR hardware and firmware functionality. *DOMHub*
705 software consists of a C-language kernel level device driver ("DOR-driver") for the DOR cards and a user-level Java
706 application called *Stringhub* on a Linux server operating system. *Stringhub's* task is facilitating the higher-level
707 configuration control and communications functions to the rest of the IceCube Surface DAQ.

708 Specific requirements for DOR-driver include the following:

- 709 • support for a few dozen control functions specific to the DOR cards,
- 710 • a clean interface between the hardware and user applications, and
- 711 • concurrent and error-free communications to all attached DOMs at or close to the maximum throughput
712 supported by the hardware.

713 The first two items are addressed by implementing a tree of control points via the Linux *proc* file system, a
714 hierarchy of virtual files used for accessing kernel functions without requiring native system calls. This somewhat
715 unusual approach allows the Java-based *Stringhub* to be written without unwieldy native interface modules. This
716 simplifies the *DOMHub* software architecture and provides the added advantage of making it very easy to operate
717 DOMs interactively or through a wide variety of test software.

718 The utilization of cyclic redundancy codes (CRCs) in the DOM-to-DOR communications stream ensures that
719 corrupt data is identified. Acknowledge/retransmit functions similar to TCP/IP in both the DOM software and in
720 DOR-driver insure that no communications packets are lost. Packet assembly/disassembly, transmit, acknowledge,
721 and retransmit are carried out on all DOMs in parallel, with periodic time calibration operations seamlessly
722 interspersed. The asynchronous activity of 8 DOR cards, 60 DOMs, multiple user applications, and many control
723 functions create substantial risk of race conditions that are identified and eliminated.

724 Extensive testing is crucial for a large device driver such as this one operating on custom hardware (in lines of
725 code, DOR-driver is comparable to a Linux Ethernet driver). The first phase of testing addresses long-term stability
726 under normal operating conditions with maximum throughput; the second phase of testing emphasizes "torture tests"
727 designed to expose unexpected races and edge conditions in the driver and firmware. Every driver-release candidate
728 must pass the verification test suite prior to deployment into production *DOMHubs*.

729

3.3.1. Communications with the DOM

730 The FPGA firmware on the DOR card contains eight instances of the communications protocol. The PCI-bus-
 731 interface FPGA relays data between the communications FPGA and the PCI bus. The half-duplex communications
 732 protocol transmits ASCII character encoded data. Transformer and capacitor coupling of the signal dictate a DC-
 733 balanced modulation. A 1 μ s wide bipolar pulse represents *logic 1*; absence of modulation represents *logic 0*. Simple
 734 threshold detection delivers satisfactory bit-error rates

735 The communications protocol includes the following commands:

- 736 • *Data Read Request*: This provides automatic data fetching from the DOMs in a round robin arbitration
 737 schema.
- 738 • *Buffer Status*: DOM/DOR data buffer synchronization, i.e. the DOM blocks DOR transmission when the
 739 receive data buffer is full. Similarly, the DOR defers data fetches from the DOM if its receive buffer is full.
 740 (When operating normally, deferred data fetches rarely result in loss of physics data as the DOM's circular
 741 data buffer can store many seconds of data.)
- 742 • *Communication Reset*: This is used to initialize the communication.
- 743 • *DOM Reboot*: This is initiated by a higher-level software command. It causes the reloading of the DOM
 744 FPGA, which results in a temporary loss and reestablishment of communication.
- 745 • *RAPcal Request*: A higher-level software command initiates a RAPcal sequence, causing the exchange of
 746 timing waveforms between DOR and DOM (about 1.5 ms duration), producing a time calibration data
 747 packet.
- 748 • *Idle*: If no data need to be transmitted to a DOM, a simple read request is transmitted. If the DOM has no
 749 data to transmit, it reports an empty queue. Absence of an expected packet constitutes a communications
 750 breakdown or an interruption, which may trigger logging or intervention.
- 751 • *CRC Error handling*: Data packets with CRC errors are not written into the receive buffer. The transport
 752 layer software is responsible for data packets retransmit. Control packets with CRC errors are ignored.
- 753 • *Hardware Timeout*: Interruption of either the data transfer or the idle packet stream for more than 4 seconds
 754 constitutes a hardware timeout. If this happens, the full system bandwidth will be utilized for
 755 communication with the remaining DOM on the pair. This feature is typically exercised when power is
 756 cycled, allowing pairs with one connected DOM to utilize the full data carrying capacity.

757

3.3.2. Stringhub

758 The Linux operating system, the top-level software element of the DOMHub₂ provides a computing environment
 759 for programs such as the *Stringhub*, which converts the flow of DOM Hits into physics-ready Hits that are suitable at
 760 both trigger and event-building stages of the surface DAQ. In principle, the *Stringhub* program can reside in a
 761 computing platform different from the DOMHub, but the DOMHub CPU is sufficient to accommodate, with
 762 adequate margin, the transformed Hit data flow rate for a string of 60 InIce DOMs or 32 IceTop DOMs.

763 The program *Stringhub* applies a time transformation to the coarse *timestamp* accompanying a Hit. These
 764 transformations bring all DOM data into a single, ICT-based time domain. Application of appropriate offsets then
 765 converts the Hit from ICT to UTC. The *Stringhub* then time orders DOM hits from multiple DOMs on a string, and
 766 can apply string-wide trigger filters.

767 The RAPcal algorithm uses data in the periodic time calibration event stream to time correct the Hit data stream.
 768 The API for time calibration has been designed to allow easy substitution of calibration algorithms as the
 769 understanding of systematic errors improves. These algorithms must achieve the correct balance between execution,
 770 speed, and accuracy. Since the converted times are only used for triggering and ordering operations, and since re-
 771 calibration of Hit times can be performed offline, algorithm performance optimizations are possible at this level.

772 Time calibration algorithms are designed to produce times with the same format and absolute reference. Each
773 transformed timestamp represents UTC time in tenths of nanoseconds since 00:00 January 1 of the year in which data
774 were acquired.

775 The *Stringhub* caches the full Hit data for later retrieval. It then creates a minimal version of each hit and sends it
776 onto the multi-string trigger handlers. When the final trigger request is sent back to a *Stringhub*, it responds with a
777 list of all hits matching the criteria and flushes all cached Hits, which occurred before the end of the time window
778 from the most recent request.

779 4. DOM Operations

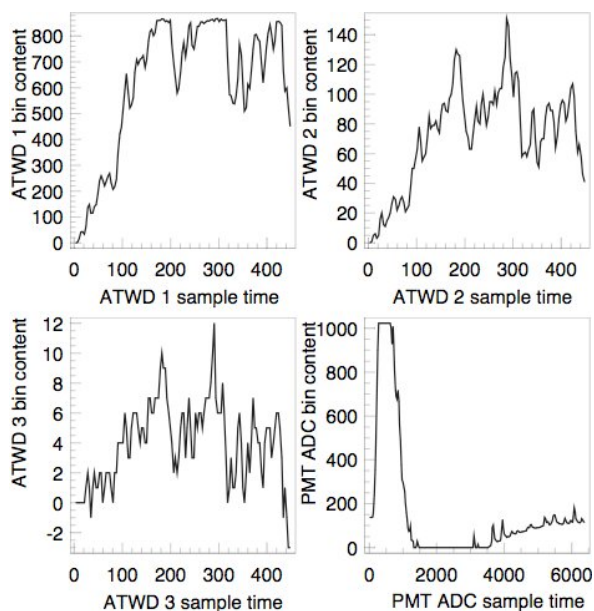
780 4.1. Hit Creation and Data Compression

781 Hits always include a 12-byte header with three distinct 4-byte components: the four-byte coarse timestamp
782 (lowest 32 bits)¹¹, the four-byte coarse charge stamp, and four bytes of trigger and housekeeping information. These
783 four bytes hold 1 bit to mark a compressed hit, 13 bits of trigger information, 4 bits to indicate the included
784 waveforms, if any, 1 bit to identify which of the two ATWDs is used for the hit, and 11 bits that show the hit size in
785 bytes. In the baseline soft local coincidence (SLC) operating mode, if a Hit has no LC tags, then no other information
786 is included.

787 When the LC condition is satisfied, the entire waveform information is transmitted. In this case, to reduce the data
788 flow, a “delta compression” algorithm is used, which exploits the fact that waveform changes from one sample to the
789 next are typically small. The delta compressor works by subtracting each sample from the preceding sample,
790 producing mostly small numbers. The differences are then encoded using 2, 3, 6, or 11 bits, with special codes used
791 to change the number of bits. For typical IceCube data, this typically compresses the waveform data by a factor of
792 3.8 without any loss of information.

¹¹ The 16 most significant bits of the timestamp change infrequently, and are hence sent once per data block to the surface DAQ, where they are reconnected to Hits. This tactic reduces the data load on the cables significantly.

793 4.2. “Slow” Waveform Capture



794

795 Figure 11. Waveforms from the three ATWD channels and the PMT ADC channel. The data were produced by light from a DOM flasher board
 796 in the ice. The horizontal scale is in nanoseconds. Since all four channels sample the same waveform, then structures in one are reflected in the
 797 others. The time behavior seen in this figure arises because the light from the flashers has different optical paths due to scattering in the ice. The
 798 different amplitudes of these structures can be explained by photon statistics.

799 Figure 11 shows the signals from all four channels from a sample Hit; the horizontal scales are in nanoseconds.
 800 Pulsing the flasher board created this Hit. The ATWD gain is highest in the top-left, medium in the top-right, and
 801 lowest in the bottom-left, while the PMT ADC signal (note the different time scale) is in the lower right. The
 802 pedestal (the value of the ATWD with no signal) has been removed from each panel. The figure shows that, when
 803 one channel saturates, more information can be recovered from a lower gain channel. The PMT ADC channel shows
 804 distortion that is the effect of a droop caused by the PMT coupling transformer. The transformer produces both an
 805 undershoot and a slow-rising waveform. This effect can be eliminated in software unless the signal drops below 0
 806 ADC counts. The short time-constant transformer used in early DOM production was later replaced with one that
 807 produces less distortion and clipping.

808 4.3. Synchronous Triggering: “Coarse” and “Fine” Timestamps

809 A high-speed comparator detects the threshold crossing of a pulse from an amplified copy of the DOM MB input.
 810 The comparator/discriminator transition time is resynchronized in the FPGA to the next well-defined edge of the
 811 DOM’s 40 MHz clock. The resynchronized, or synchronous, trigger signal launches ATWD capture, and
 812 simultaneously latches the DOM’s clock counter value (“Hit time”) on the next clock edge. Synchronous triggering
 813 eliminates the possibility of ± 1 count timestamp errors when trigger transitions occur near a clock edge. The latched

814 value of the DOM's 48-bit local clock counter constitutes the coarse timestamp for that Hit. As the DOM local clock
815 runs at 40 MHz, the leading edge of the PMT signal can appear anywhere within a fixed 25 ns window within the
816 ATWD record. The coarse timestamp thus measures Hit time with about 7 ns RMS resolution, which is more than
817 adequate for trigger formation and time ordering of data.

818 For physics analysis purposes, better time resolution is desired for Hits with waveform data. The determination,
819 *ex post facto*, of the position of the leading edge of the PMT waveform within the ATWD record provides a "fine
820 timestamp", with a resolution better than the 3.3 ns ATWD sample rate, and well within the 4 ns RMS system
821 requirement.

822 4.4. Local Coincidence Modes

823 The Local Coincidence (LC) capability is realized by connecting each DOM to its nearest neighbor with a
824 dedicated bidirectional, duplex links (transceivers) over copper-wire twisted-pairs. The LC feature permits DOMs to
825 transmit and receive LC "tag" messages to and from DOMs above or below. A DOM that receives an LC tag can
826 modify and propagate the message further, thereby establishing an LC coincidence length (maximum distance
827 between DOMs contributing to a LC tag).

828 The local coincidence hardware consists of a pulse generator coupled to a power splitter. The center port of the
829 power splitter connects to the transmission line matching circuit for the off-board twisted pair. The power splitter
830 topology makes possible simultaneous transmission and reception of LC signaling at each DOM. The transceivers
831 support data rates in excess of 10 Mbps, transmitting an LC packet in 350 ns over links ranging from 21 m to 55 m.

832 When a Hit occurs, a DOM opens a receptive time window, which is typically not more than one μ s. If during this
833 window, a tag signal is received from a neighbor DOM, then the local coincidence requirement will be satisfied.
834 Conversely, if a quiescent DOM, *i.e.*, one that is not currently processing a Hit, receives a tag signal from a neighbor,
835 then it will also establish an identical receptive time window to accommodate the possibility that it may also receive a
836 Hit. The processing of LC signals by the DOMs is thus time symmetric, so that LC tag creation does not bias against
837 the time order of Hits. Conversely, FPGA firmware can adjust the window offsets to allow either upward-going or
838 downward-going muons to be favored; neither option is exploited.

839 Hit information includes the presence or absence of tag signals from neighboring DOMs. Tagged Hits occur at a
840 few percent of the total PMT rate (depending on the coherence length), and are much more likely to have been
841 created by a particle than by PMT noise. An LC tag thus provides an immediate and efficient data selection criterion.

842 Beyond various testing and commissioning modes of operation, there are only two basic modes of array operation
843 that employ local coincidence signals: "Soft" (SLC) and "Hard" Local Coincidence (HLC). There is a third trigger
844 condition, Self-Local Coincidence (self-LC) that only relies upon a single DOM.

845 4.4.1. Soft Local Coincidence

846 In SLC, the baseline-operating mode of IceCube, only those Hits with an LC tag will contain PMT ADC and
847 ATWD waveform data; untagged (isolated) hits contain no ATWD waveform data. In SLC operation, the LC tag rate
848 is typically ~ 10 Hz, depending strongly on depth of a DOM from the surface, and on the chosen coherence length.
849 The DOM thus digitizes ATWD signals much slower than the ~ 700 Hz PMT SPE rate.

850 The justification for SLC is that isolated Hits are about two orders of magnitude more likely to be PMT noise
851 pulses than physics event signals. Thus, the SLC mode significantly reduces both the dead time, and the recorded
852 data flow from noise Hits, while sacrificing only a small fraction of real Hit waveforms.

853 *4.4.2. Hard Local Coincidence*

854 HLC requires every Hit to have an LC tag. This allows a high level of background rejection and reduction in data
855 flow by discarding all PMT triggers without LC tags. In HLC, isolated Hits are lost. In addition, DOMs on either
856 end of the string and DOMs with non-functioning neighbors suffer reduced trigger efficiency. This operating mode is
857 used during commissioning and initial science operations.

858 *4.4.3. Self-Local Coincidence*

859 Self-LC provides for a DOM to include ATWD waveform information in the Hit when the PMT pulse is
860 significantly larger than a characteristic single pe pulse in that DOM, even in the absence of received LC tags. The
861 two PMT discriminators have thresholds that can be set independently. While one discriminator's threshold is
862 always set to a fraction of a PE, the second discriminator's trigger threshold can be set to trigger on substantially
863 larger pulses, which occur rarely. Triggering of the second discriminator initiates self-LC hit processing, without
864 adding excessively to the data flow. This mode of operation can coexist with SLC or HLC.

865 Self-LC could also be built into the ATWD readout engine. Resources in the FPGA can be configured to
866 recognize signatures that are more complex.

867 *4.5. Coarse Charge Stamp*

868 Monte Carlo simulations show that events do cause isolated hits, and therefore, some extra information about
869 charge (i.e., about the number of photoelectrons collected in a time window) is useful in global trigger formation or in
870 event categorization/reconstruction down stream from the *Stringhub*. To provide this extra information, but with
871 minimum impact on data flow, an FPGA firmware module constructs a coarse charge stamp from a snippet of the
872 PMT ADC record. Every Hit includes a coarse charge stamp, regardless of LC tag.

873 The 32 bits allocated for this purpose are arranged to include the highest ADC sample within the first 16 samples
874 (400 ns) plus the immediately prior sample and subsequent sample. Only nine bits of the three ADC samples are
875 selected. Another bit specifies the range. Depending on signal amplitude, either the most significant or least
876 significant nine bits are chosen. The four remaining bits specify the index of the highest ADC sample with respect to
877 the beginning of the record.

878 *4.6. DOM Dead time*

879 In the baseline SLC mode of operation, dead time is expected only within individual DOMs. No dead time is
880 anticipated to occur due to data transfers from DOMs or due to any messaging activity. Due to the autonomous
881 nature of DOM operation, dead time is distributed throughout the array with negligible inter-DOM correlations.

882 No dead time is incurred while a DOM is capturing waveform information. However, if ATWD digitization is
883 initiated once the capture phase is over, dead time may occur, depending on the instantaneous circumstances.
884 Because Hits are always created during such occurrences, the dead time intervals are known and can be taken into
885 account during reconstruction of the candidate events. The DOM mitigates dead time in two ways:

- 886 1. Use of Local Coincidence: Both SLC and the more restrictive HLC permit ATWD digitization only for those
887 Hits with LC tags. The LC tag rate for Hits with a coincidence length of two is in the range of 2 to 15 Hz, a
888 factor of ~ 100 less than for a mode requiring no tags for digitization. This reduces ATWD dead time
889 substantially. Note that every trigger initiates ATWD waveform acquisition. However, processing by the Hit
890 readout engine in the FPGA is aborted at the end of the LC window when no neighbor LC tag is received.

891 Afterwards, the DOM is ready for the next trigger in 50 ns. The rate variation tracks the optical properties of the
892 ice, as the rate is highest where the ice is most transparent.

893 2. Use of two ATWDs: Analog to digital conversion by the ATWD requires 29 μs per channel. As each DOM
894 contains 2 ATWDs, should a DOM retrigger after 6.4 μs while one ATWD is digitizing, the other ATWD is
895 available to start another Hit capture sequence. In SLC mode, a dead time of 50 ns (2 clock cycles) occurs at the
896 end of the local coincidence window during the state transition to the alternate ATWD. Furthermore, a dead time
897 of up to 22.5 μs is accrued if the second ATWD is launched before the first is read out completely. The latter
898 case occurs at roughly 1 Hz. Thus for a random 500 Hz trigger rate, the dead time is $\sim 1 \times 10^{-5}$. However, the
899 dominant sources of PMT noise pulses in the DOMs are scintillations in the glass pressure sphere and the PMT
900 glass, due to ^{40}K and U-Th decays. These produce a correlated fluorescent emission as much as ~ 1 ms later.
901 Dead time is hence increased relative to a random flux. We estimate that the total dead time fraction does not
902 exceed $\sim 1 \times 10^{-4}$. A firmware module in the FPGA counts clock cycles whenever the DOM is neither acquiring
903 data nor ready for a trigger. Thus, the in situ dead time can be precisely measured, but this task has not yet been
904 done.

905 4.7. Reciprocal Active Pulsing (RAPcal)

906 The RAPcal method coordinates an ensemble of over 5000 free running clocks with respect to a GPS disciplined
907 reference to establish a common time-base for all Hit data. It has a sequence of six distinct steps that determine the
908 instantaneous frequency and phase (or offset) of the DOM's local clock relative to the Master Clock on the surface.

909 The steps are as follows:

- 910 1. The DOR card commands the DOM to enable the RAPcal time-calibration sub-process; the DOM acknowledges
911 receipt of command and enters a quiescent receptive state. However, PMT signals continue to be captured,
912 digitized, and buffered.
- 913 2. After the DOM acknowledges readiness, the DOR sends to the DOM a precisely timed bi-polar pulse, the
914 RAPcal signal. At the source, the transition edge rise- and fall-time is 5 ns and is synchronized with the system
915 clock to better than 100 ps. The DOR card firmware latches the value of the 56-bit clock counter exactly when
916 the RAPcal signal begins. The pulse amplitude and width are chosen to produce a robust received signal after
917 attenuation and dispersion in the cable.
- 918 3. The DOM's firmware senses the arrival of the dispersed, attenuated pulse as a digital threshold crossing in the
919 communication ADC data stream. The DOM records the entire pulse waveform, plus a few samples of baseline
920 prehistory. The DOM clock-counter value associated with the last pulse waveform sample becomes the coarse
921 time stamp of this portion of the RAPcal record.
- 922 4. To insure a quiet condition on the cable, the DOM's RAPcal firmware initiates a short, fixed length idle period
923 "8" before proceeding.
- 924 5. The DOM's firmware then generates its response to the DOR, a pulse identical in shape to the initial DOR pulse.
925 The DOR's firmware senses and timestamps the pulse's arrival as the DOM did in (3) above. (This near-identity
926 of received time-calibration pulse shapes, within natural variations due to components, is termed reciprocal
927 symmetry.)
- 928 6. The DOR then requests the pulse waveform and time stamped data from the DOM. The two transmit times, the
929 two received waveforms, and the two received times constitute the complete RAPcal record.

930 The data from the above steps enable a linear transformation from DOM local time to ICT for all Hits. Identical
931 fiducial points are set for each received waveform, e.g., a leading edge or the crossover point of a bipolar pulse, as in
932 Figure 12. These points define the time a pulse is received - a local time if received by a DOM, an ICT time if
933 received at the DOR. The ratio of time intervals ΔT_{DOR} between successive pulses transmitted by the DOR and the

934 local time intervals ΔT_{DOM} at which the DOM receives these pulses determines the ratio of master and local clock
 935 frequencies:

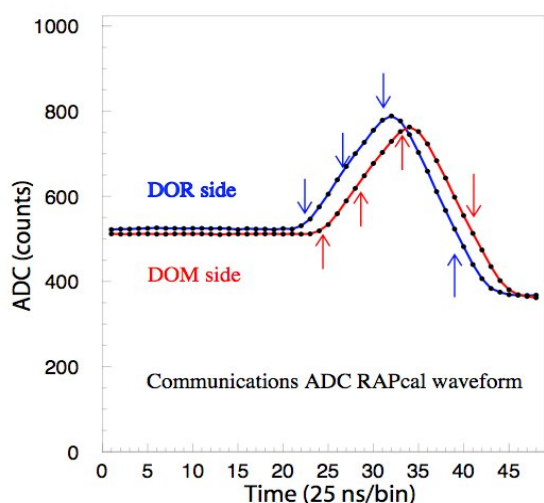
$$936 \quad v_{\text{local}}/v_{\text{master}} = \Delta T_{\text{DOR}} / \Delta T_{\text{DOM}}$$

937 The offset of the local clock with respect to the master clock (the difference in clock values at the same instant of
 938 time) can be determined once the one-way propagation time τ is known for a calibration pulse sent between DOR and
 939 DOM. Reciprocal symmetry, or the identity of pulse shapes, results in identical values of τ for pulses sent in each
 940 direction. The value of τ can therefore be determined from a measurement of the round trip time (ρ) minus the
 941 known "idle period" (δ) regardless of which waveform feature is taken as the fiducial point:

$$942 \quad \tau = 1/2 (\rho - \delta)$$

943 Reciprocal symmetry is verifiable because the calibration waveforms are digitized in both the DOM and the DOR,
 944 and the waveforms, like those in Figure 12, can be compared to determine if any important differences in shape are
 945 present. Simple estimators, such as extrapolation of the nearly linear part of leading edge or crossover region to
 946 baseline, the midpoint along the leading edge, or a centroid approach, provide precision on the order of 1-2 ns RMS.
 947 Repetitive measurements quickly make statistical errors for τ negligible.

948 Beyond any possible second-order effects arising from temperature gradients along the 3 km cable, the effects of
 949 possible asymmetries resulting from differing electrical component values, different temperatures at the DOR and
 950 DOM, and the impedance asymmetry introduced by compression of the quad cable, or the unterminated stub at one
 951 DOM were studied on the laboratory bench top by phase locking a DOM's local clock to a DOR card's local clock.
 952 Asymmetry effects were, at most, at the level of 0.1 to 0.2 ns, consistent with measurement error. Any remaining
 953 asymmetries that are common to all DOMs and DORs would affect only the offset between ICT and UTC.



954
 955 Figure 12. A typical RAPcal waveform, with 4 different time marks (arrows). The top curve (blue or DOR side) on the left is measured at the
 956 DOR, while the other (red or DOM side) is measured at the DOM. The time positions of the waveforms were adjusted so they could be easily
 957 compared.

958 The timing precision is limited by electrical noise on the cable and can be estimated by a simple relationship
 959 between electrical noise and rise-time:

960 $\delta t \sim \delta V / (dV/dt)$,

961 where δV is the RMS noise/error voltage, and dV/dt is the received pulse rise time, ~ 160 mV/ $0.6 \mu\text{s}$. From the
962 observed timing precision and pulse rise-time, the inferred noise voltage is ~ 0.7 mV, which is slightly higher than
963 the communications ADC quantization error of 0.4 mV. Because RAPcal is intrinsically sensitive to high frequency
964 electrical noise, care was taken in the design of circuitry, cables, and operation to minimize induced noise. Since the
965 time calibration procedure is repeated at regular intervals, individual calibrations that have been substantially affected
966 by noise are easily recognized and discarded. In that case, the previous calibration is used for an additional
967 calibration interval.

968 The RAPcal interrogation rate needed to track the oscillator drift in each DOM depends on the actual stability,
969 which is expected to vary somewhat for each oscillator. Typically, the measured DOM oscillator drift under stable
970 temperature conditions is remarkably good, with $\delta f/f < 3 \times 10^{-11}$. This permits interrogation intervals of a minute, or
971 perhaps more, before drift has accumulated to a magnitude that would affect off-line event reconstruction. However,
972 intrinsic oscillator frequency drifts and phase fluctuations display occasional, minute, abrupt discontinuities. In
973 current practice, the time calibration sequence takes less than ~ 1.4 ms, and is set to occur once per second. The time
974 spent in time calibration is hence invisible to the main task of data flow.

975 The coarse timestamp (cf. Section 4.3) is useful for triggering purposes, and is corrected by extrapolation, i.e., by
976 using the two previous RAPcal events. In subsequent data analysis, it is possible to use the events just before and just
977 after the photon's arrival, i.e., by interpolation. At this time, this correction is not needed as the current method
978 provides sufficient precision.

979 The ice surrounding the DOMs constitutes a massive, stable heat sink for their crystal oscillators. However, on
980 power-up after an extended off period, the oscillators are subject to a $\sim 10^\circ\text{C}$ temperature rise due to heating from the
981 3.5W dissipated by DOM MB electronics and the PMT HV power supply module within the glass sphere enclosure.
982 Once in steady-state operation, the ensemble of all oscillators in IceCube constitutes a very stable virtual clock,
983 whose stability is expected to exceed by a wide margin the short- and medium-term stability of the GPS receiver,
984 which is affected by algorithmic discontinuities and an evolving mix of satellite signals.

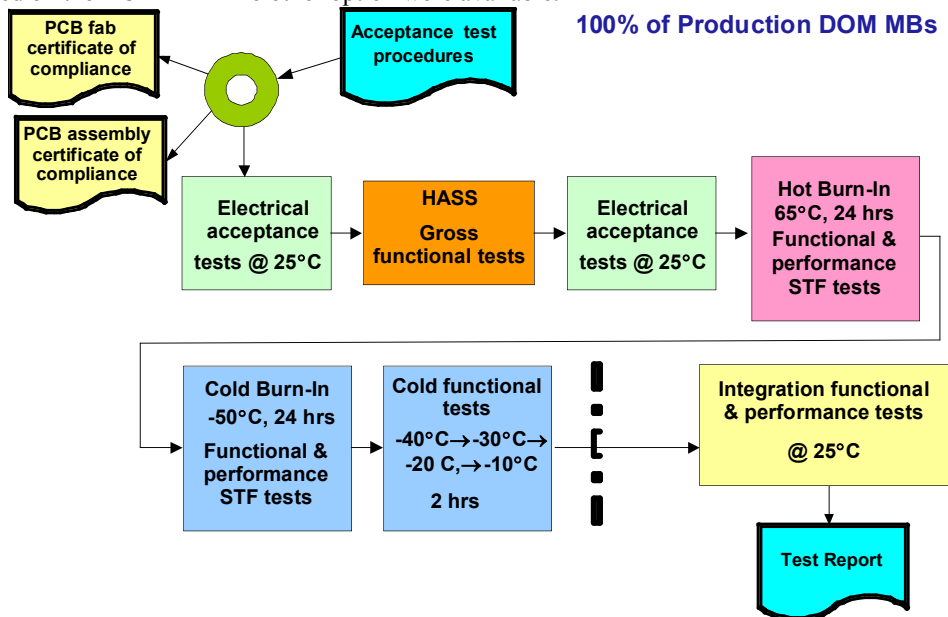
985 RAPcal requires distribution to the DOMHubs of GPS-derived signals with sub-nanosecond synchronization, and
986 highly coordinated actions in both DOM and DOMHub. The real-time nature of the RAPcal process dictates that
987 code is implemented in firmware, rather than software. The RAPcal data set, acquired repetitively, is sufficient to
988 establish a rolling time transformation of DOM time to ICT.

989 5. DOM MB Manufacturing and Testing Procedures

990 Because a deployed DOM cannot be repaired, stringent manufacturing and testing procedures were obligatory to
991 minimize failure of a DOM MB during deployment and after it becomes frozen in the ice. The design goal is that not
992 more than 5% of the DOMs shall fail within 10 years of operation, where failure is defined as complete loss of
993 physics-useful data. A quality control program was developed to support the achievement of this goal. The design
994 strategy centered on understanding how, where and why failures occur in boards and associated components when
995 exposed to the operational conditions encountered in IceCube. A flow chart describing the production of the DOM
996 MB can be seen in Figure 13.

997 The design and fabrication philosophy addressed failure propagation, supplier selection, manufacturing quality
998 level, material restrictions, design control, and configuration control. The power and communications input circuit
999 on the DOM MB is designed to maximize the probability of an open circuit (rather than a short or low-impedance
1000 circuit) in the event of a catastrophic board failure. This enables the neighboring DOM on the same wire pair to

1001 continue operating. Where possible, the electronic parts were selected from manufacturers that had been vetted by
 1002 NASA and the Department of Defense as suppliers of high quality components. All components used are required to
 1003 operate either in the Industrial (down to -40°C) or, preferably, MIL (down to -55°C) temperature range. The
 1004 component's temperature range depended on availability and cost. Material restrictions minimized inclusion of
 1005 materials with properties that could potentially shorten the life of the sensors. For example, plastics incompatible
 1006 with low temperature, cadmium, pure tin, and zinc plating are not appropriate for critical applications, and were only
 1007 used on the DOM MB if no other option were available.



1008
 1009 Figure 13. DOM MB production flow. The steps to the left of the dashed-dotted line were done at an outside vendor, while the steps to the right
 1010 were performed at LBNL.

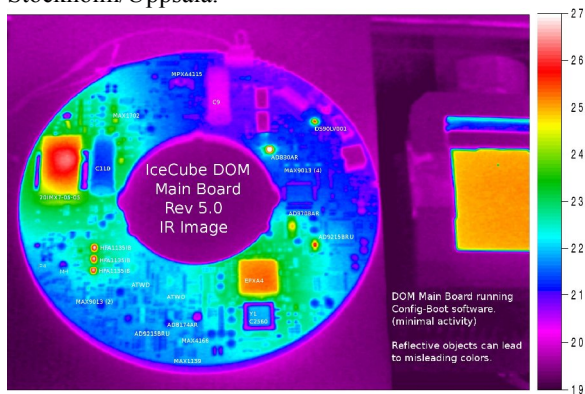
1011 Design, management, and manufacturing controls were put in place to guarantee a consistent product that would
 1012 meet all system and manufacturability requirements over several separate procurement cycles. DOM design
 1013 verification was based principally on testing because it provides the highest level of confidence that the actual
 1014 performance meets the specified requirements. As testing of some requirements such as a life of 10+ years was not
 1015 practical, verification was done by analysis. Design reliability was addressed by subjecting a sample of pre-
 1016 production DOM MB assemblies to a stress test method called Highly Accelerated Life Time Test (HALT), which
 1017 exposed the DOM MB to extremes in vibration and temperature cycling while operational.

1018 The test regimen consisted of a cold and hot temperature stress, rapid thermal transitions, a vibration stress step, and
 1019 finally simultaneous temperature cycling and vibration. During all portions of the HALT testing, the DOM MB was
 1020 monitored continuously by running the STF suite. The final result of HALT testing confirmed the suitability of the
 1021 DOM MB design.

1022 The DOM MB was imaged thermally to determine if there were any excessive hot spots that could cause later
 1023 failures. The image that is shown in Figure 14 indicates that there is a localized approximate 5°C rise due to heating

1024 in the DC-DC converter in an open environment. This figure also shows the power dissipated by the active
 1025 communications components, the EPXA4, and wide-band amplifiers.

1026 A test stand was used to subject each manufactured DOM MB to an extensive series of tests to be sure that they
 1027 also met specifications. First, every manufactured DOM MB was tested for function and performance at room
 1028 temperature, using the STF suite of tests. Following that, the next stage in the DOM MB test process was a less
 1029 stressful version of HALT, called Highly Accelerated Stress Screening (HASS). HASS was used to test performance
 1030 from -40°C to $+65^{\circ}\text{C}$ and vibration to 5G. Following HASS, all DOM MBs were tested at $+65^{\circ}\text{C}$ for 24 hours and $-$
 1031 50°C for 24 hours. In the next testing stage, the DOM MB was connected to a PMT, a High-Voltage Base board, a
 1032 Flasher board, and 2500 m of twisted quad cable to test all system interfaces. After a DOM MB assembly passed all
 1033 these production tests, it qualified to be integrated into a DOM at assembly sites in Wisconsin, Berlin, or
 1034 Stockholm/Uppsala.



1035
 1036 Figure 14. This is an infrared image of a DOM MB that was operating for about 40 minutes. The orange block on the right hand side is a
 1037 reference temperature source in units of centigrade. Some of the objects in the picture appear colder because they reflect surrounding areas.

1038 The last stage in the production test cycle was to load sealed DOMs into a Deep Freezer Lab (DFL), and run a
 1039 Final Acceptance Test (FAT) on all units. The FAT lasted 3 weeks, including slow temperature cycles from 25°C to
 1040 -45°C , periodic STF tests, and a Calibration test suite, all under the control of a test DAQ system. About 85% of the
 1041 DOMs passed these FAT tests. Failures arose from malfunctions from any of the sub-components.

1042 Once a DOM passes all of these tests, it was ready for shipment to the South Pole. After arrival at the South Pole,
 1043 it was tested again, to detect any damage during shipment. At this point, the DOM was ready to be deployed into the
 1044 IceCube array.

1045 6. Performance

1046 The operation of IceCube to August 2008 allows a first assessment of IceCube's performance. Tests of the DAQ
 1047 in situ, as well as normal operation, which involve communicating with deployed DOMs, measure the performance
 1048 of the communications hardware and protocols. The ability of IceCube to identify point sources of neutrinos, should
 1049 they exist, depends on the pointing resolution of reconstructed muon trajectories. The pointing resolution depends
 1050 quadratically on angular reconstruction accuracy, which in turn depends on time resolution for detecting the

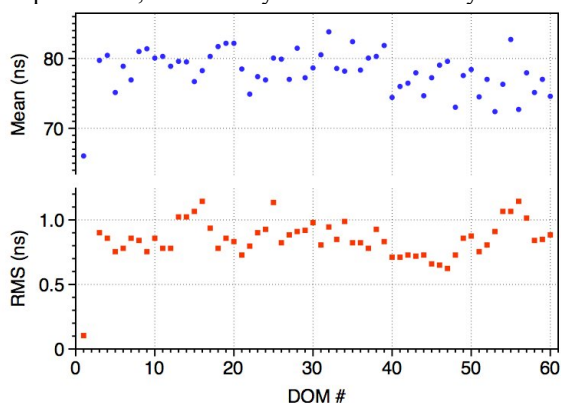
1051 Cherenkov radiation. Despite the degrading impact of optical scattering by the ice, some photons are nearly “direct”,
 1052 and their accurate detection is particularly important. Accordingly, time resolution requirements of 4 ns RMS for
 1053 individual DOMs and 7 ns RMS for the entire IceCube DAQ system were established to ensure that technical aspects
 1054 would not compromise information quality.

1055 6.1. Timing

1056 The accuracy with which the system can determine the time of arrival of a photon at the photocathode has been
 1057 determined from flasher calibration sources and cosmic ray muons.

1058 6.1.1. Timing with Flashers

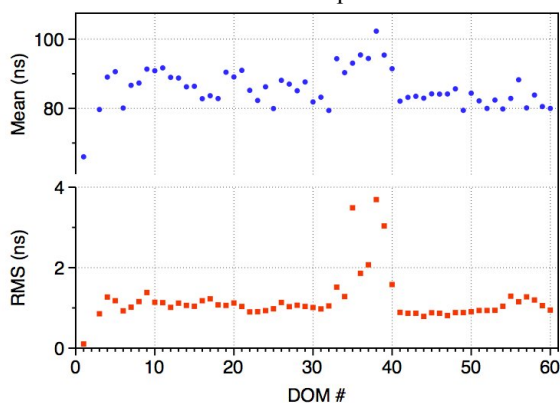
1059 A straightforward test of the system in ice is to pulse the LEDs on the flasher board at a known time and measure
 1060 the arrival time of photons at an adjacent DOM on the same string. Since this measurement depends on the accuracy
 1061 of the time calibration procedure for both the emitting DOM and the receiving DOM, stochastic errors will combine
 1062 in quadrature, but some systematic errors may be more difficult to detect.



1063
 1064 Figure 15. A plot of the mean and the RMS of the difference in time between flashing an LED and arrival of the photons at the receiving DOMs.
 1065 The flashing DOM is located below the receiving one. The top graph (blue) shows the mean values, while the bottom (red) shows the RMS
 1066 deviation. DOM 1 is at the top of the string, while DOM 60 is at the bottom. The mean includes the time that the light propagates in the ice.

1067 Figure 15 shows the mean times and RMS values for optical signals received by a DOM when the flashers in the
 1068 DOM below it are operated. The distance between DOMs (17 m) is small enough that the first photons from high
 1069 intensity light flashes experience little or no scattering. Thus, time calibration and the response of the DAQ
 1070 electronics, and not the scattering properties of the ice, should dominate the resolution. Since many photons are
 1071 detected in a short time, the single-photon timing response of the PMT should not contribute much to the time
 1072 residuals. As this test measures the difference in time between the LED flash (as determined by calibrating the clock
 1073 in that DOM) and first photon’s arrival at the second DOM (as determined by calibrating the clock in that DOM), the
 1074 actual resolution for a single DOM is $1/\sqrt{2}$ of the measured resolution if the dominant contribution to the resolution is
 1075 error in time calibration.

1076 Most of the RMS values for 59 DOMs in this particular string are less than 1.5 ns (RMS), which indicates that the
 1077 time calibration error and any other stochastic contributions to the resolution are 1 ns or less. In these tests, the
 1078 ATWD is used to determine the photon arrival time.



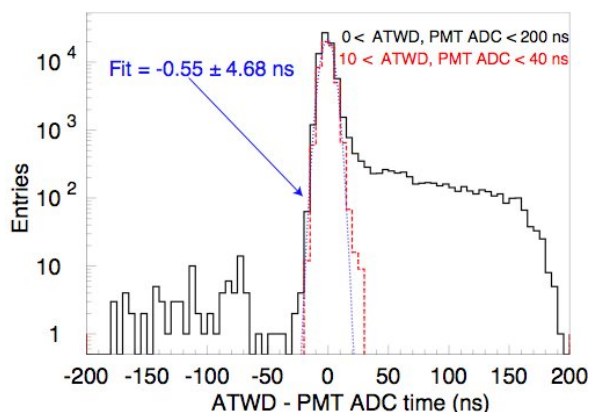
1079
 1080 Figure 16. The RMS and mean time difference between photons arriving at two adjacent DOMs located just above a third, flashing DOM. The
 1081 top graph (blue) shows the mean values, while the bottom (red) shows the RMS deviation.

1082 Systematic errors in timing that involve the properties of the LED flashing system can be eliminated by using two
 1083 adjacent DOMs to receive light emitted by the flashers on a third DOM located below the two receiving DOMs. The
 1084 difference in arrival times of photons received in the upper two DOMs emitted in the same light burst is independent
 1085 of the absolute time at which the burst occurs. The distance traveled by photons to the farthest DOM is now 34 m,
 1086 which provides additional opportunity for photons to be scattered in the ice with a corresponding delay and jitter in
 1087 the arrival time. Therefore, the measured time distributions will correspond to upper limits on the time resolution of
 1088 the system. A $1/\sqrt{2}$ factor applies here as well in estimating the resolution for an individual DOM. The results of
 1089 such a test are shown in Figure 16. The increase in both the time and the time resolution for DOMs, which are
 1090 numbered between 33 and 40, arises from a dust layer in the ice[13].

1091 The arrival time of a photon is normally determined from the ATWD waveform. The PMT ADC also records the
 1092 waveform. Since the ATWD and ADC simultaneously capture the first 420 ns after a trigger, both devices can be
 1093 cross calibrated.

1094 The ATWD sampling rate is calibrated by making a measurement (using STF and a diagnostic input channel of
 1095 the ATWD) of the sampling clock used for the PMT ADC. The sampling time offset for the ATWD with respect to
 1096 the PMT ADC is measured by injecting a short light pulse generated by an on-board LED into the PMT, then
 1097 measuring the arrival time in both the ATWD and ADC.

1098 Figure 17 shows that the time resolution for the ADC is just under 5 ns, and that the average arrival time for
 1099 photons determined with these two methods agrees to within 0.6 ns. The observed resolution, 4.7 ns, is about 20% of
 1100 the bin width for the PMT ADC, which is comparable to the relative resolution seen in the ATWD.



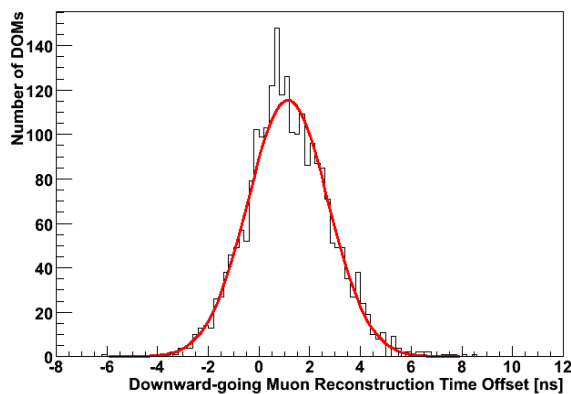
1101

1102 Figure 17. The time difference for pulses reconstructed in both the ATWD and PMT ADC. This difference is -0.6 ± 4.7 ns, dominated by the
 1103 ADC's resolution. The solid (black) curve is plotted for ATWD and ADC sampling in the range between 0 and 200 ns. The dashed (red) curve
 1104 has a narrower range of 10 to 40 ns.

1105 6.1.2. Timing with muons

1106 The flux of down-going cosmic ray muons penetrating the active volume of the IceCube array enables a test of the
 1107 timing performance of the DOMs under the same conditions as actual data-taking. Even when imposing cuts, it is
 1108 possible to perform this timing test with high counting statistics at regular intervals throughout the year.

1109 First a muon track is reconstructed using all hits except for one "test DOM" to avoid any bias in the fit. The
 1110 predicted arrival time from this track is then compared with the measured arrival time of the photon at the "test
 1111 DOM". Despite the limited accuracy of the track position measurement, the requirement that the reconstructed track
 1112 passes within 15 meters of the "test DOM" minimizes the effects of scattering in the ice. This procedure of
 1113 eliminating one DOM from the reconstruction is repeated for the set of DOMs that are sufficiently close to the muon
 1114 track.

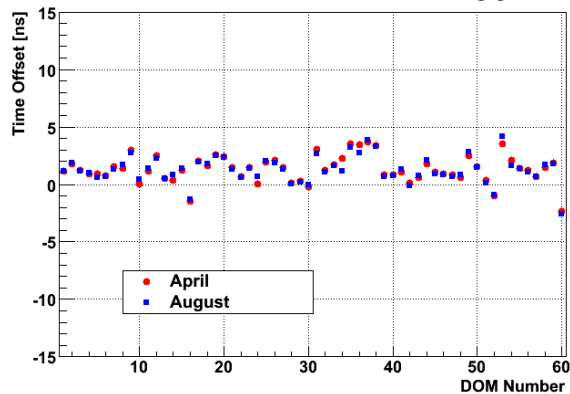


1115

1116 Figure 18. The peak values of the difference between the predicted time (based on fitted muon tracks) and the measured photon arrival time for the
 1117 active 2341 InIce DOMs out of a total of 2400. This measurement was taken in August 2008. The width, σ , of the Gaussian fit is 1.6 ns.

1118 Figure 18 shows the distribution of the peak values of the difference between the predicted and measured arrival
 1119 times for the active 2341 out of the 2400 InIce DOMs. This distribution is narrowly peaked at 1.1 ns with a variation
 1120 of 1.6 ns.

1121 This method also can be used to study the stability of the time calibration. Figure 19 shows the results from data
 1122 taken in April 2008 and again in August 2008 for a typical string (String 48). The measured time shift for each DOM
 1123 was found to be less than 1.0 ns, demonstrating good stability over several months of operation.

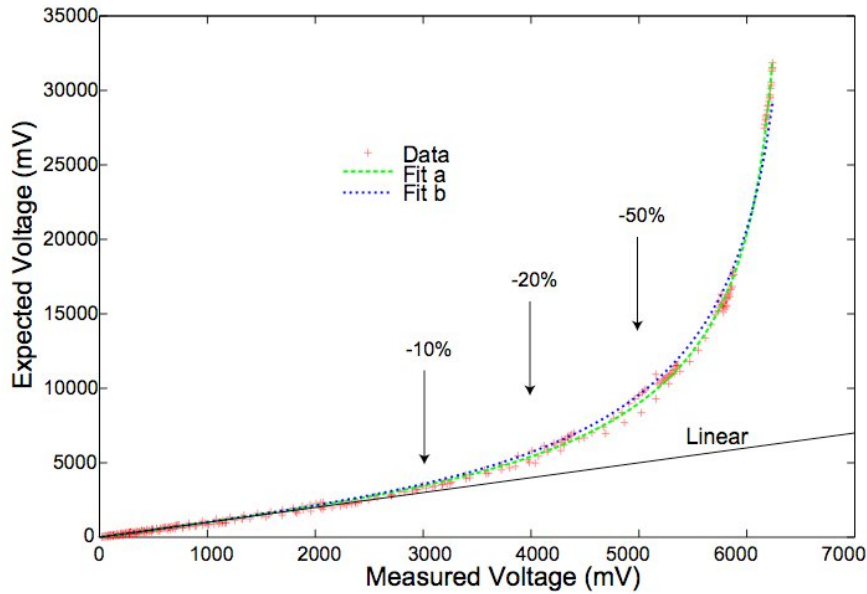


1124
 1125 Figure 19. The peak values of the time distribution for the 60 DOMs on String 48 were measured in April 2008 (red circles) and again in August
 1126 2008 (blue squares). For all DOMs, the difference between these two sets of date is less than 1.0 ns.

1127 6.2. PMT Linearity Measurement

1128 The PMT SPE signals are well calibrated at a known nominal gain of 1×10^7 . Accurate measurement of the
 1129 number of photons arriving at a DOM thus translates to the measurement of charge. The charge is given by
 1130 calculating the area of the waveform peak. The measurement of charge will be affected by the linearity of the
 1131 electronic signal path for different gains. This can be checked by determining the area of a pulse that falls in a region
 1132 covered by two ATWD gain stages and comparing the results. This test shows that the calibration of the different
 1133 ATWD channels is sufficiently accurate to determine pulse height over a wide dynamic range using the LED flashers.
 1134 Since each DOM contains 12 independently operable LEDs, linearity can be determined by observing the response to
 1135 individual LEDs, operating one at a time. Once the individual response is known, the response to varying numbers of
 1136 LEDs pulsed simultaneously can be measured and deviations from linearity determined.

1137 Figure 20 shows the results of such a test for a typical PMT. The deviation from linearity reaches 10% at ~ 400
 1138 photoelectrons/15 ns. Of course, calibrating the response of the PMT in the non-linear region and making the
 1139 appropriate corrections for larger pulses can extend the dynamic range extended beyond 1000 photoelectrons/15 ns.



1140

1141 Figure 20. PMT linearity that has been measured for one phototube.

1142 *6.3. Temperature Variation*

1143 IceCube DOMs are deployed in varying thermal environments, which potentially affects instrument response.
 1144 InIce DOMs could be subject to a systematic position dependant calibration, while IceTop DOMs may experience
 1145 temporal changes. As described in Section 5, DOMs are tested and calibrated over the full range of IceTop and InIce
 1146 temperatures. Once deployed, InIce DOMs experience a constant temperature and the calibration needs only to be
 1147 done at the operating temperature at a fixed location. The timing behavior is constant throughout the year as
 1148 demonstrated by Figure 19. IceTop presents special challenges. The overall change in IceTop DOM launch rates are
 1149 of order 20%, of which 15% is associated with day-to-day changes of barometric pressure, which modulates the flux
 1150 of secondary particles produced in air showers. There remains a 10% seasonal variation that may be due to structural
 1151 changes of the upper atmosphere, the response of DOM to changing local temperatures, or some other cause. These
 1152 issues will be discussed in subsequent papers.

1153 *6.4. Reliability*

1154 By the end of the fourth operational year of IceCube, 2560 DOMs had been installed. Twelve of them, 0.5% of
 1155 the total, are not useable, having failed during deployment or freeze-back of the borehole ice. Evidence suggests that
 1156 most of these failures were due to stresses on cables and connectors during freeze-back. Three InIce DOMs and one
 1157 IceTop DOM failed after the ice froze. One of these appears to have failed due to loss of PMT vacuum, as indicated
 1158 by a pressure decrease in the DOM.

1159 The DOM MB electronics failure rate after deployment – at most 3 in 3260 DOM years – during this notably short
1160 operational period suggests that some 97% of the full complement of DOMs may survive in 25 years. This survival
1161 rate is much higher than the previously stated design goal of 95% in 10 years. In any case, the relatively small
1162 number of failures so far is encouraging and likely attributable to the extensive quality assurance program.

1163 Beyond this relatively small number of failures, there are some 30 DOMs that have minor problems and are
1164 temporarily "out of service" but should return to useful operation. At any given time during operation of the IceCube
1165 InIce array for data taking, 97% - 98% of the deployed DOMs are operating according to specification. The
1166 performance for IceTop DOMs is comparable.

1167 7. Summary

1168 The IceCube DOM MB evolved from the circuit board developed for AMANDA's prototype DOMs. This
1169 experience and several newly available components prompted the selection of a more integrated, higher performance
1170 CPU-FPGA implementation, a more robust and flexible independent local coincidence transceiver, and a more
1171 sophisticated higher performance mezzanine card flasher subsystem interface. The prototype DOM's CPU fetched 8-
1172 bit event data from the FPGA's memory, whereas the DMA engine in the IceCube FPGA transfers 32-bit data into the
1173 CPU's memory. This change delivers much higher performance with reduced CPU load, resulting in a data rate
1174 nearly double that of the prototype DOMs. The DOM's modular real-time software design provides an increased
1175 functionality and robustness for a modest increase in resource usage. Since the IceCube DOM's flash file system
1176 stores multiple programs and FPGA configuration files, the DOM MB's operating system transitions between them as
1177 needed for data acquisition and periodic system testing. To enhance noise suppression in the HV subsystem, a serial
1178 DAC and ADC on the mezzanine card replaced the HV analog control. The DOR card and DOMHub were
1179 significantly redesigned to improve the performance and packing density and facilitate scaling the system to 80
1180 strings. In addition, there were numerous other improvements that resulted in a very reliable system that can be
1181 duplicated many thousands of times.

1182 These improvements produced a DOM MB, which controls all the functionality within the DOM. The DOM MB
1183 communicates digitally with the surface by a single twisted pair of copper wires. The main functions of it are PMT
1184 signal (waveform) capture and digitization, timestamping of Hits, calibration, coincidence logic, communications,
1185 and monitoring. The design and the performance of the DOM, first extensively tested and verified in the laboratory,
1186 meet the science-driven design requirements for operation in the deep ice and on the surface in the IceTop tanks. A
1187 comprehensive quality assurance and testing program maximizes the probability that deployed DOMs will perform as
1188 required. So far, the DOMs are performing very well, with a failure rate (including all sources of failure) of about
1189 1%. On average, 98% of all deployed DOMs participate in experimental data taking for physics purposes. Almost
1190 all of the DOM failures are due to cable or deployment issues.

1191 Acknowledgments

1192 We acknowledge the support from the following agencies: U.S. National Science Foundation-Office of Polar
1193 Program, U.S. National Science Foundation-Physics Division, University of Wisconsin Alumni Research Foundation,
1194 U.S. Department of Energy, and National Energy Research Scientific Computing Center; Swedish Research Council,
1195 Swedish Polar Research Secretariat, and Knut and Alice Wallenberg Foundation, Sweden; German Ministry for

1196 Education and Research, Deutsche Forschungsgemeinschaft (DFG), Germany; Fund for Scientific Research (FNRS-
1197 FWO), Flanders Institute to encourage scientific and technological research in industry (IWT), Belgian Federal
1198 Science Policy Office (Belspo); the Netherlands Organisation for Scientific Research (NWO); M. Ribordy
1199 acknowledges the support of the SNF (Switzerland); A. Kappes and A. Groß acknowledge support by the EU Marie
1200 Curie OIF Program. Throughout the conception, design, and building of this system, W. Chinowsky has provided
1201 invaluable advice and guidance. Michael Phipps and the University Program of Altera Corporation provided us with
1202 samples, development tools, advice, and technical support. We also thank the engineering and technical staff at
1203 Lawrence Berkeley National Laboratory who were essential to the design, construction and testing of the DOM MB.

1204 **References**

- 1205 [1] A. Achterberg *et al.*, *Astropart. Physics* 266 (2006) 155.
1206 [2] J. Ahrens *et al.*, IceCube Preliminary Design Document, (2004). <http://www.icecube.wisc.edu/science/publications/pdd/>.
1207 [3] F. Halzen & D. Hooper, *Repts. Prog. Phys.* 65 (2002) 1025.
1208 [4] J. Learned & K. Mannheim, *Ann. Revs. Nucl. Part. Sci.* 50 (2000) 679.
1209 [5] J. Ahrens *et al.*, *Phys. Rev. D* 66 (2002) 032006.
1210 [6] E. Resconi for the IceCube Collaboration, arXiv:0807.3891.
1211 [7] R.G. Stokstad, for the IceCube Collaboration, published in the 11th Workshop on Electronics for LHC and Future Experiments, Sept. 12-16,
1212 2005, Heidelberg, Germany.
1213 [8] M. Ackermann *et al.*, *Nucl. Instru. and Meth. A* 556, (2006) 169.
1214 [9] S. Kleinfelder, *IEEE Trans. on Nucl. Sci.*, **50** No. 4 (2003) 955.
1215 [10] R.G. Stokstad, D.M. Lowder, J. Ludvig, D. Nygren, and G. Przybylski, LBNL-43200 (1998).
1216 [11] See <http://tf.nist.gov/timefreq/service/gpstrace.htm> and <http://tf.nist.gov/timefreq/time/oneway.htm>.
1217 [12] See <http://sourceware.org/newlib/>.
1218 [13] M. Ackermann *et al.*, *Journal of Geophysics Research*, 111, (2006) D13203.

Figure 1
[Click here to download high resolution image](#)

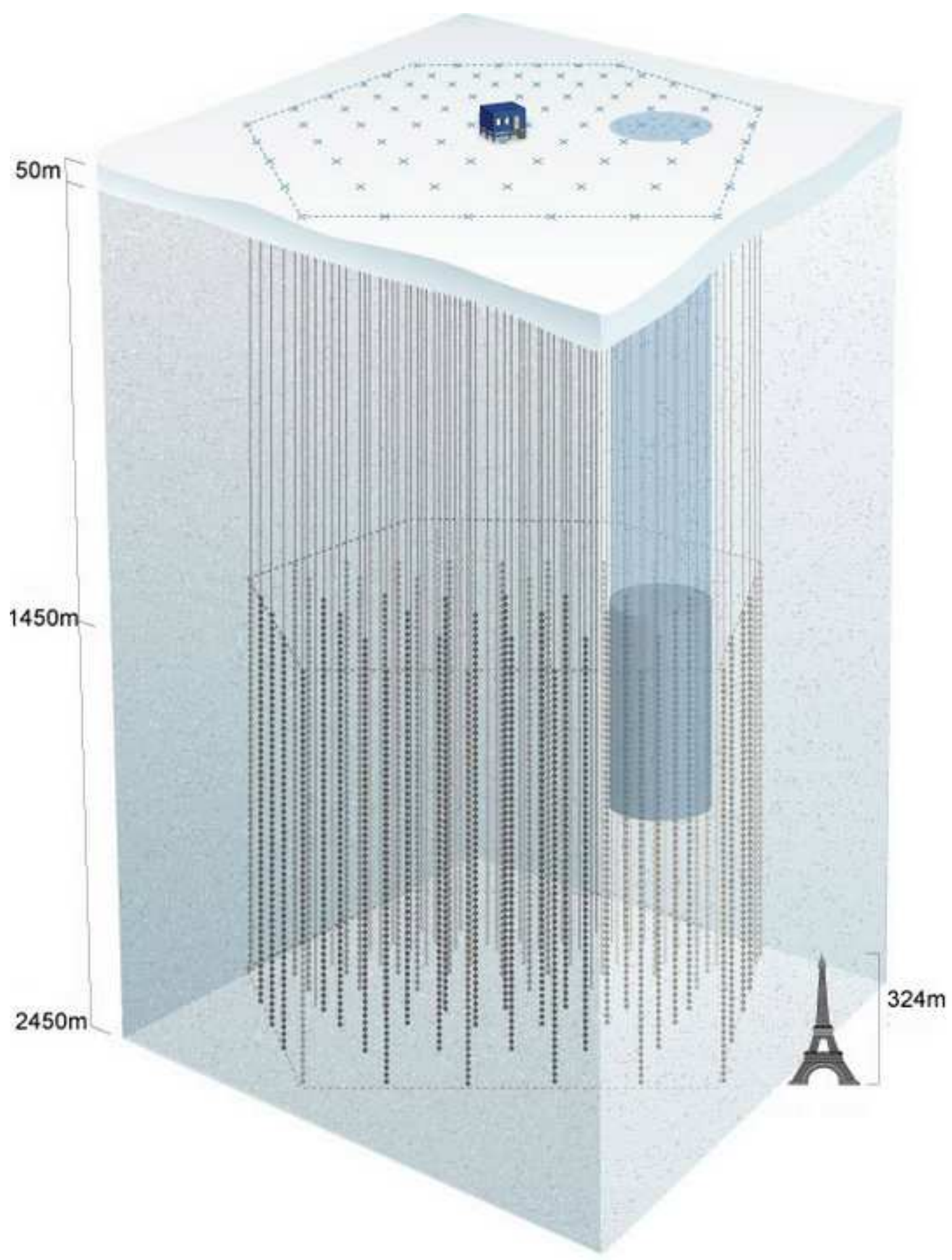


Figure 2
[Click here to download high resolution image](#)

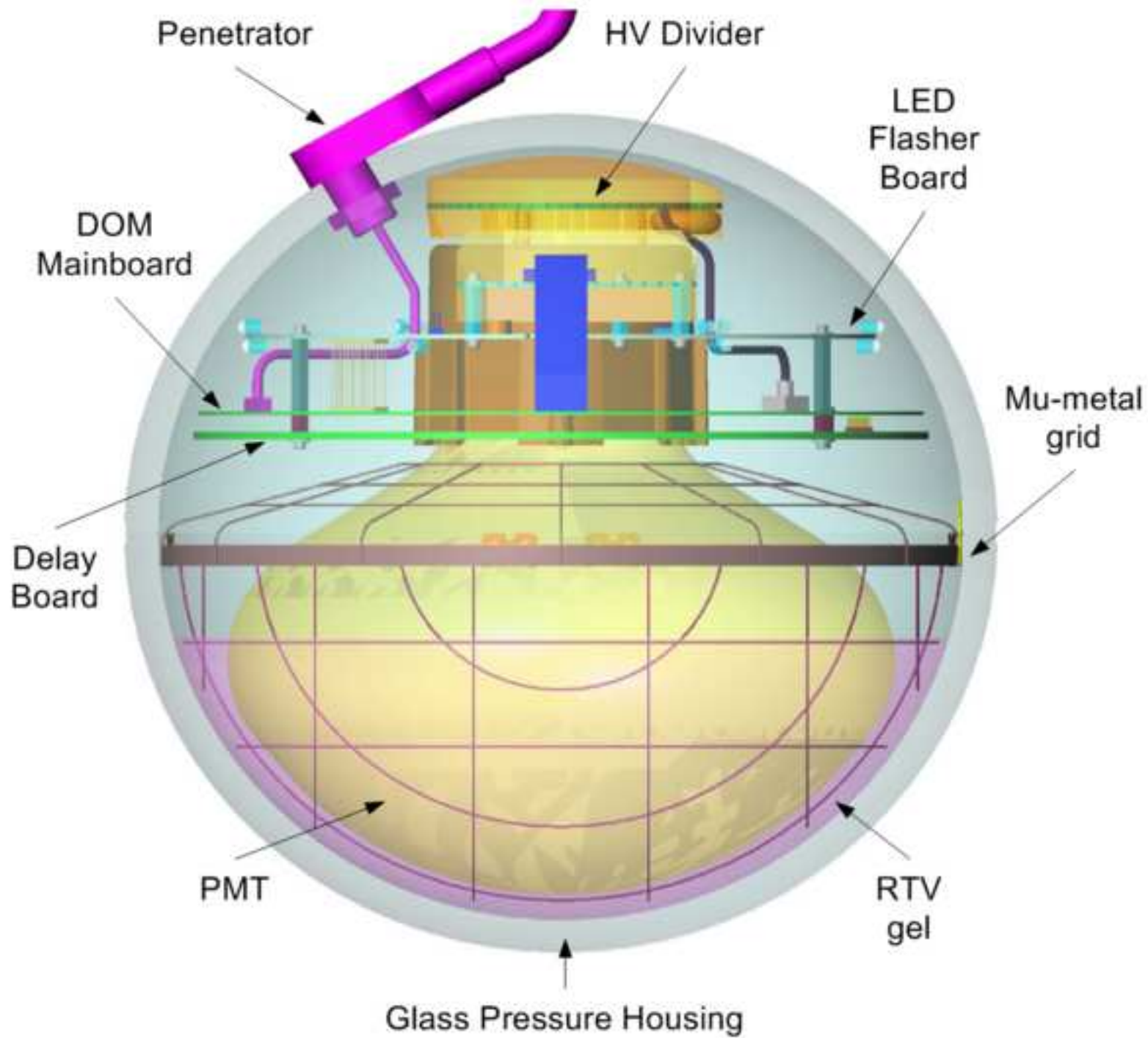
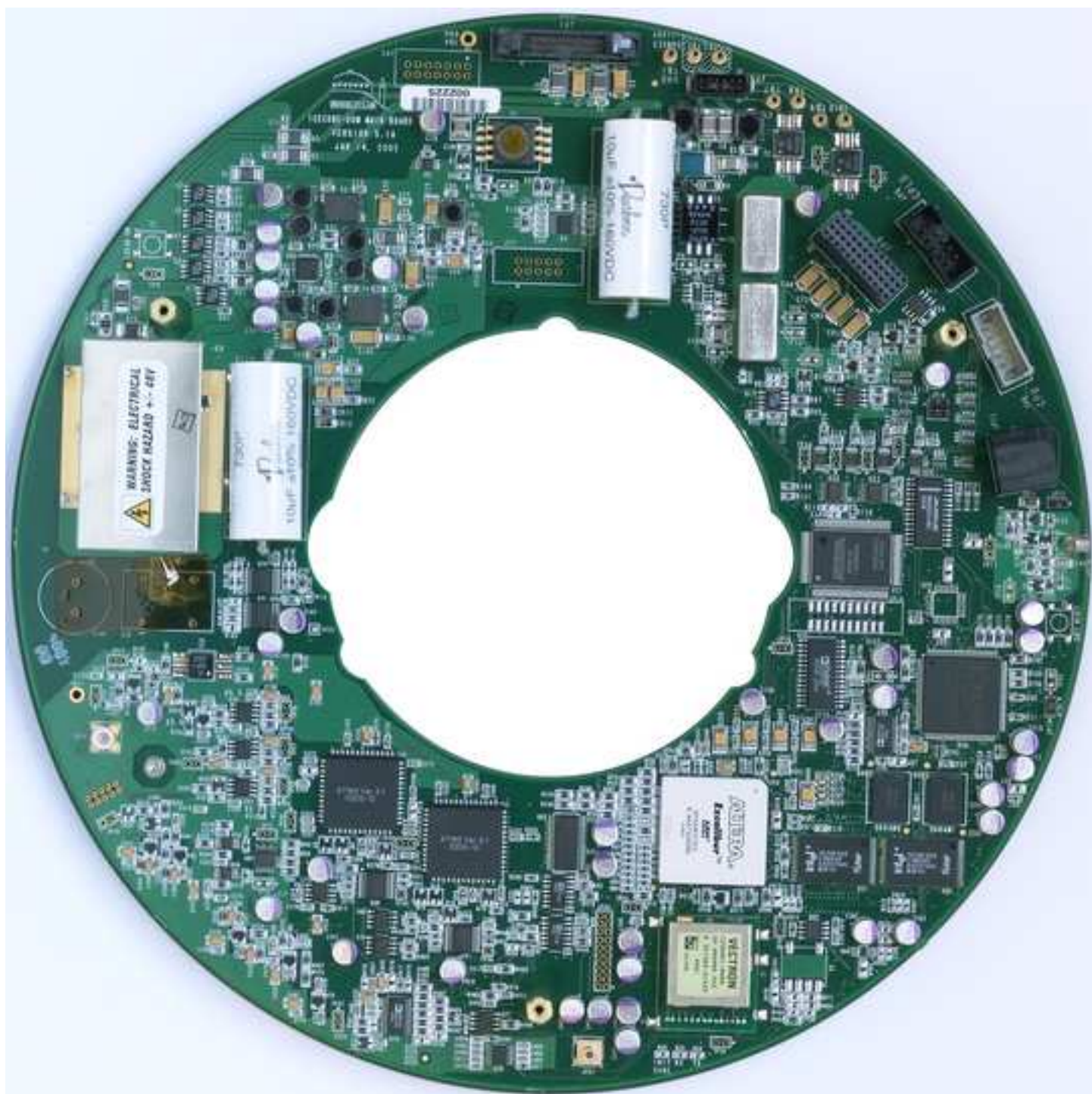


Figure 3
[Click here to download high resolution image](#)



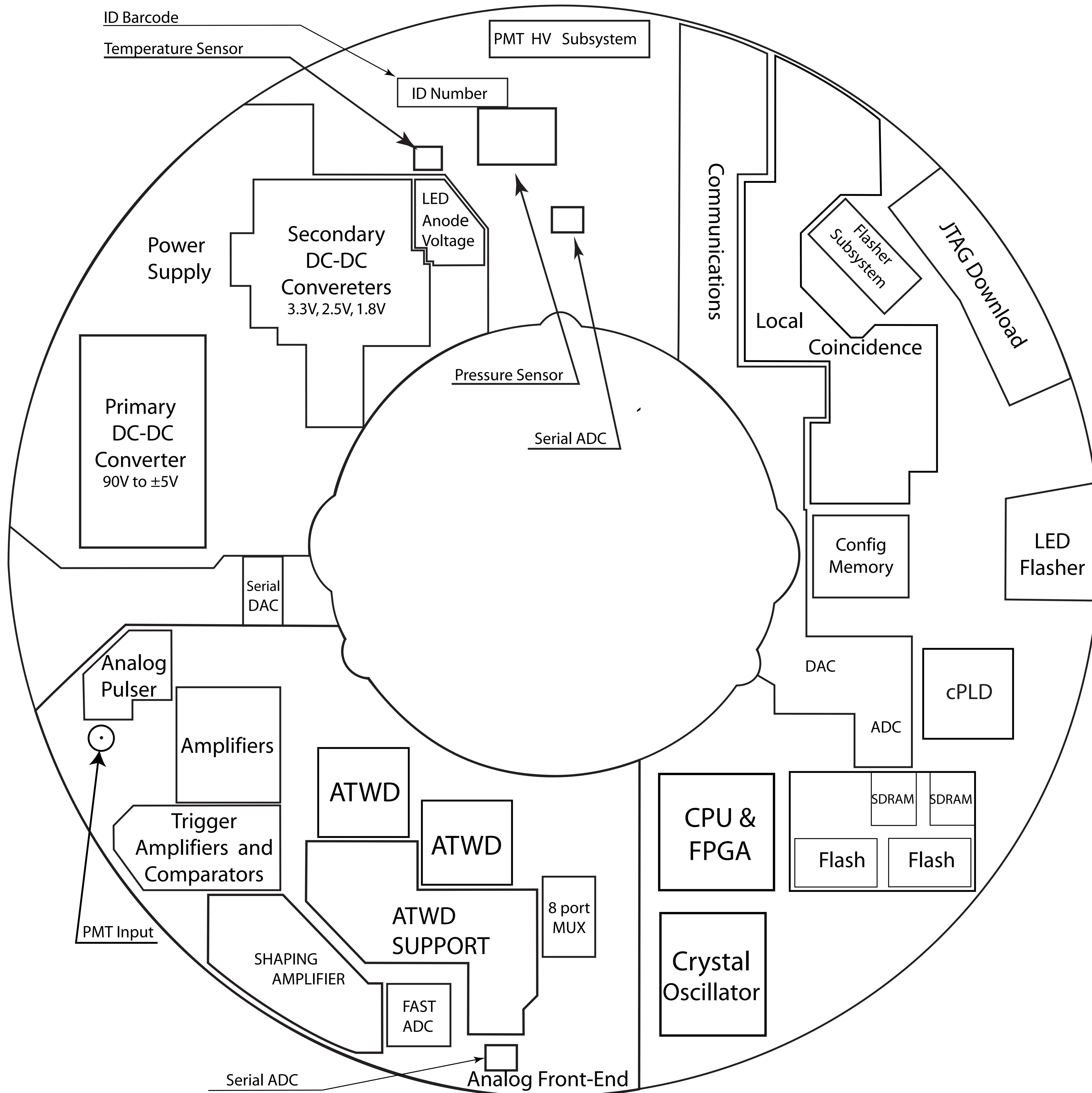


Figure 5

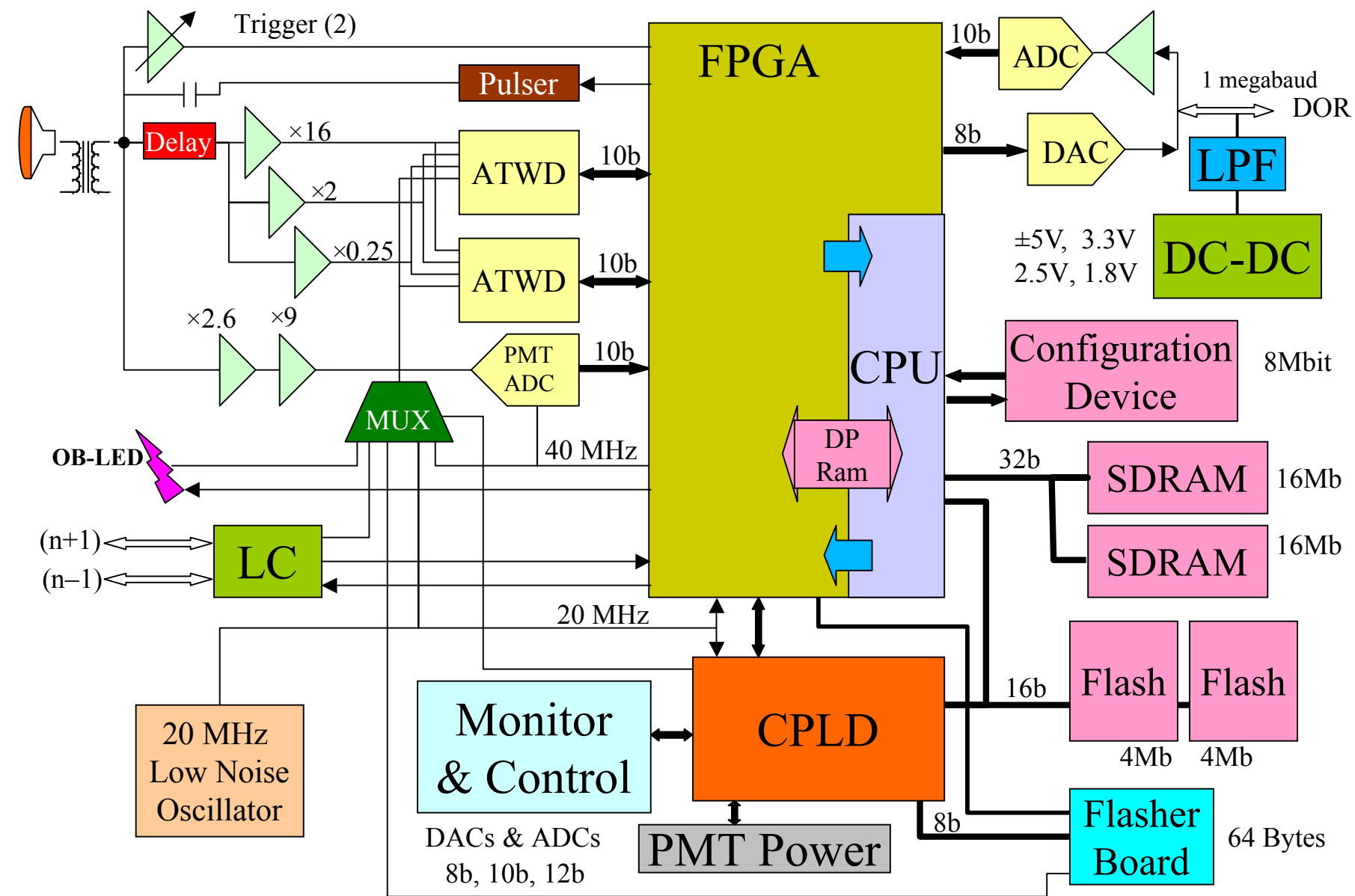


Figure 6
[Click here to download high resolution image](#)

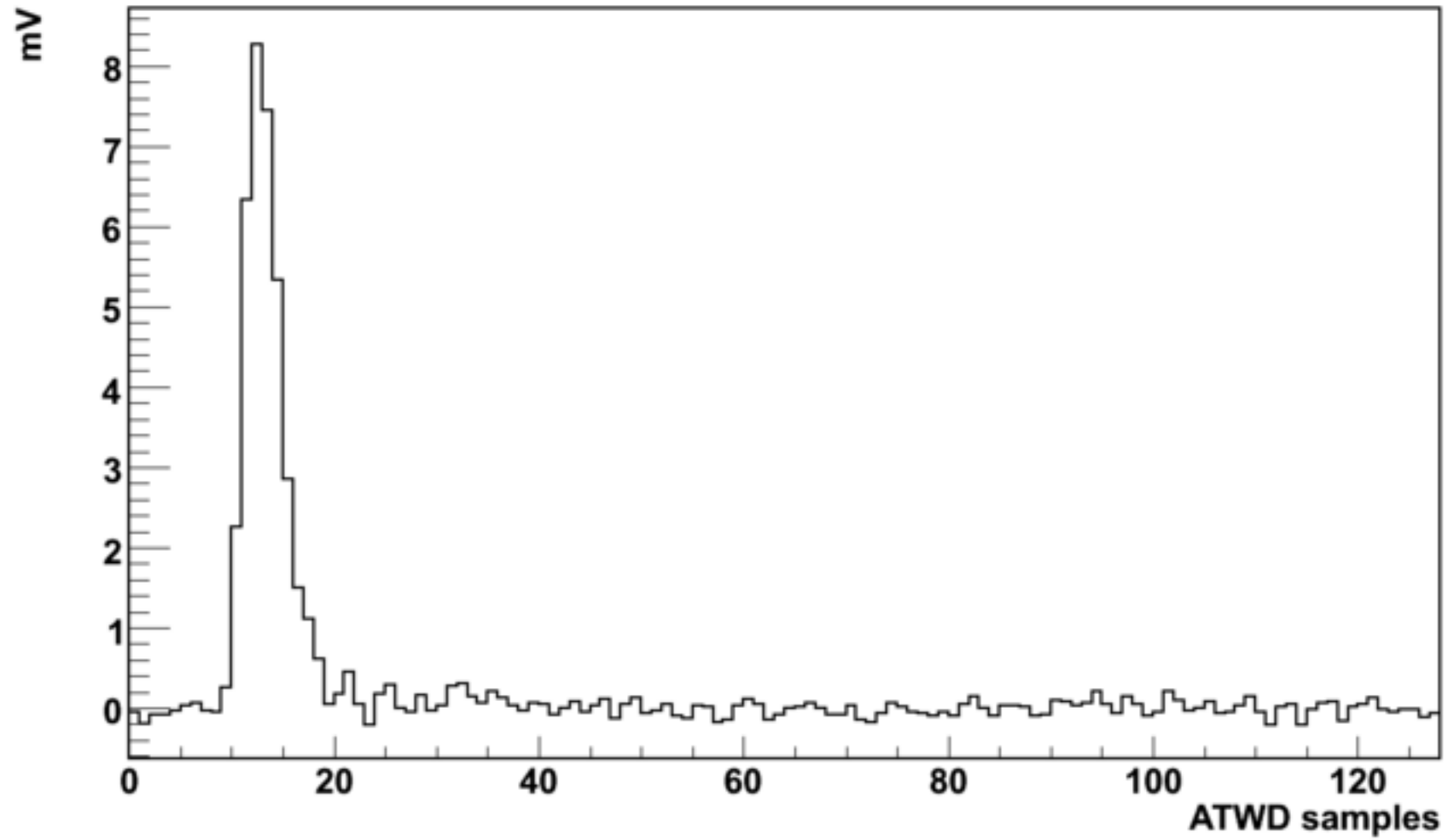


Figure 7

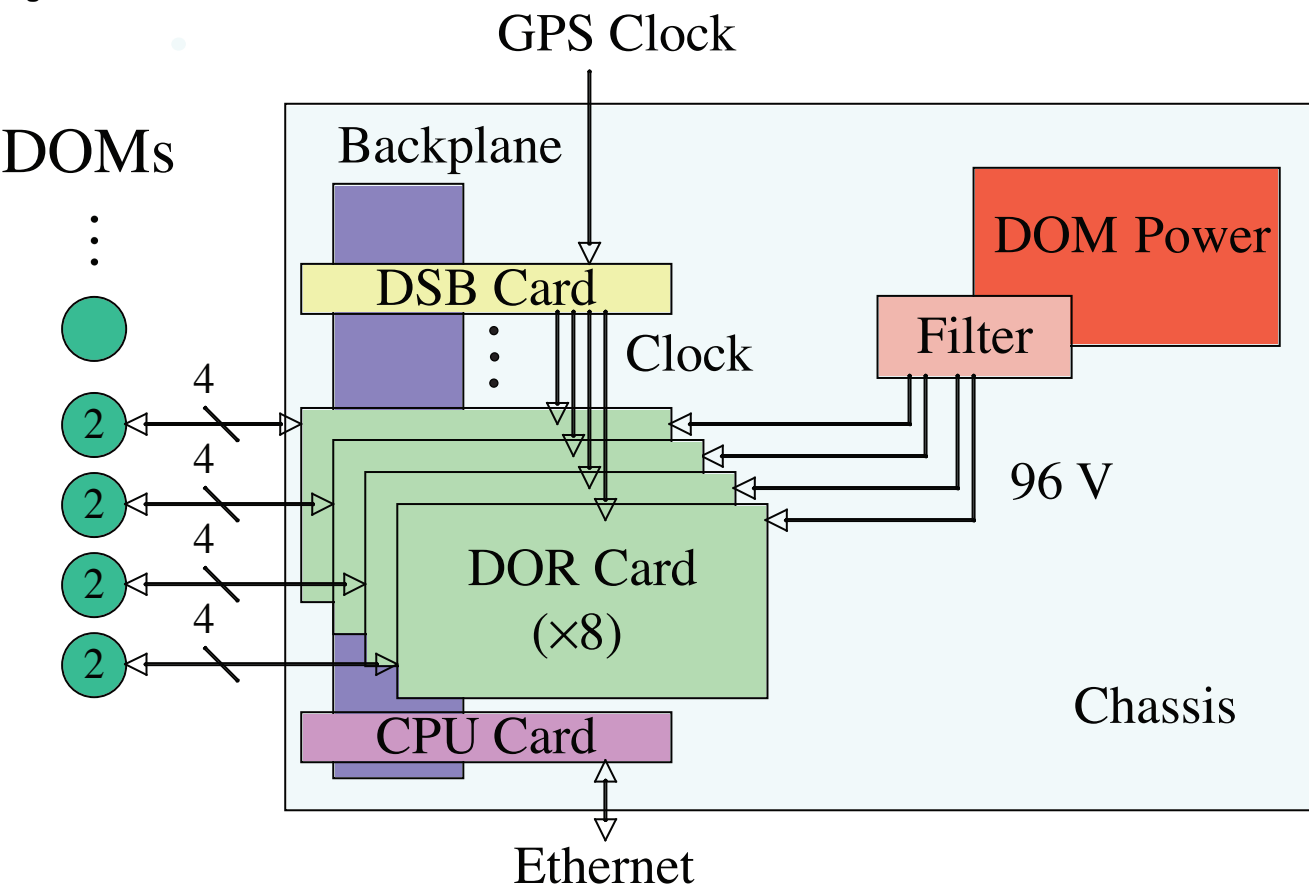


Figure 8
[Click here to download high resolution image](#)

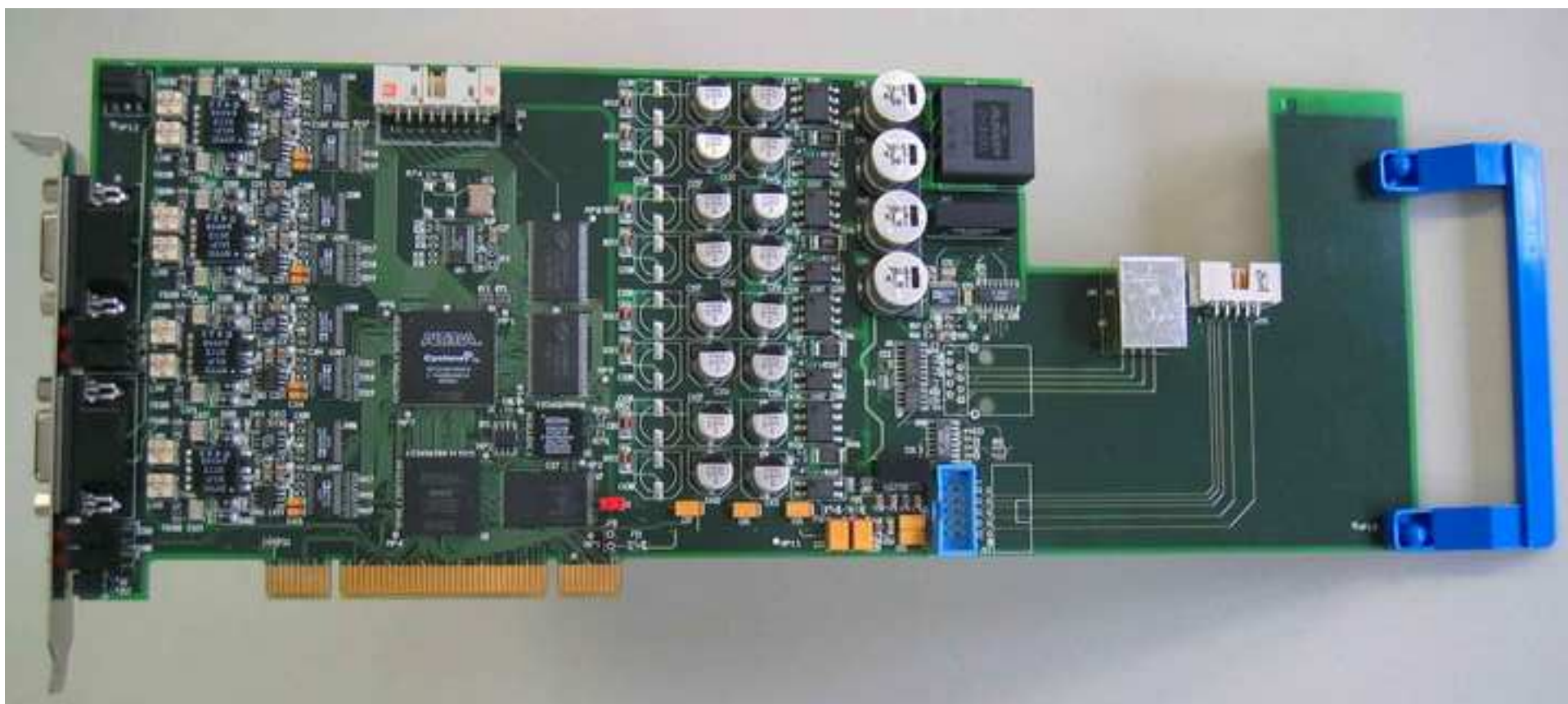


Figure 9

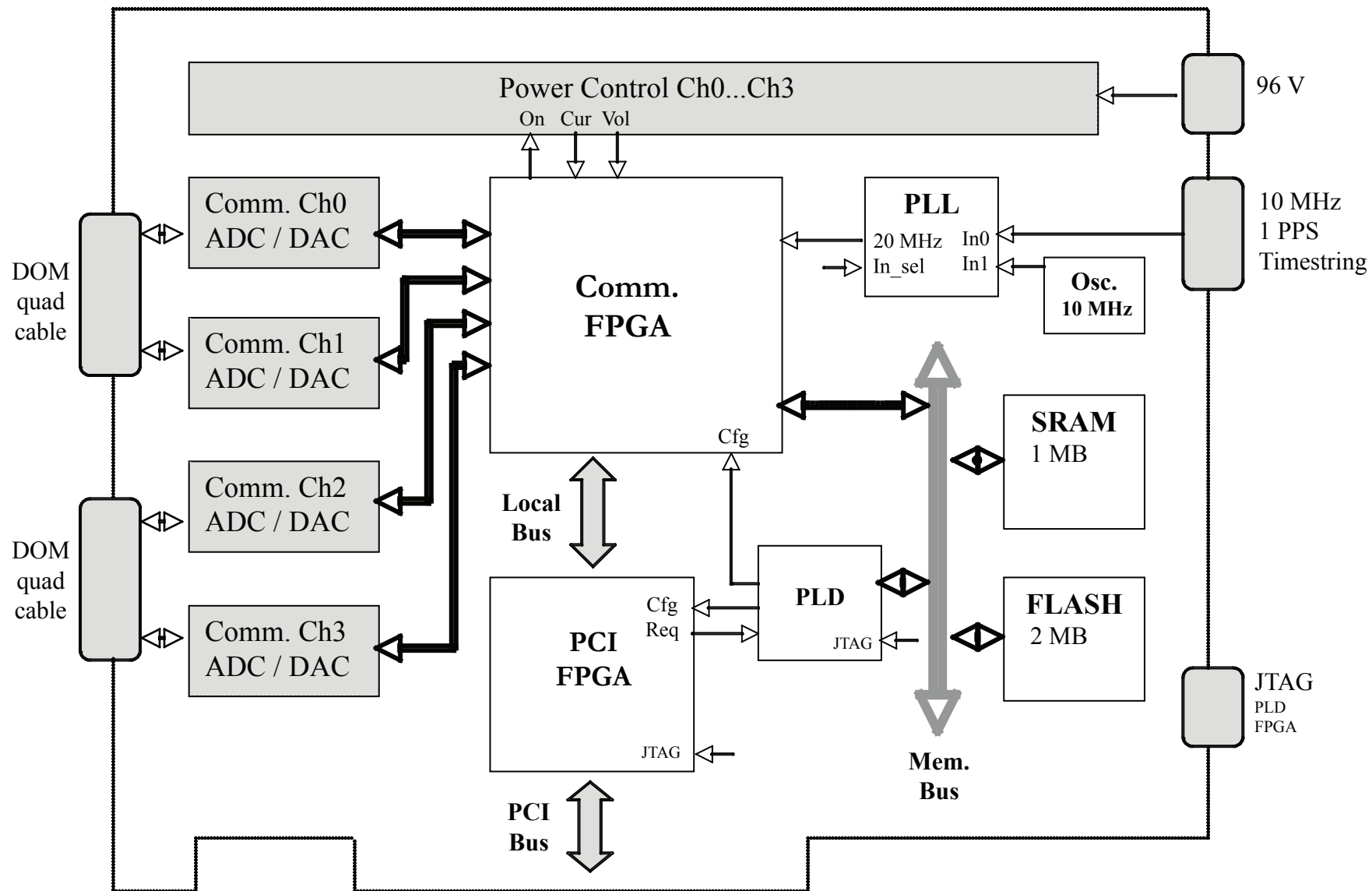
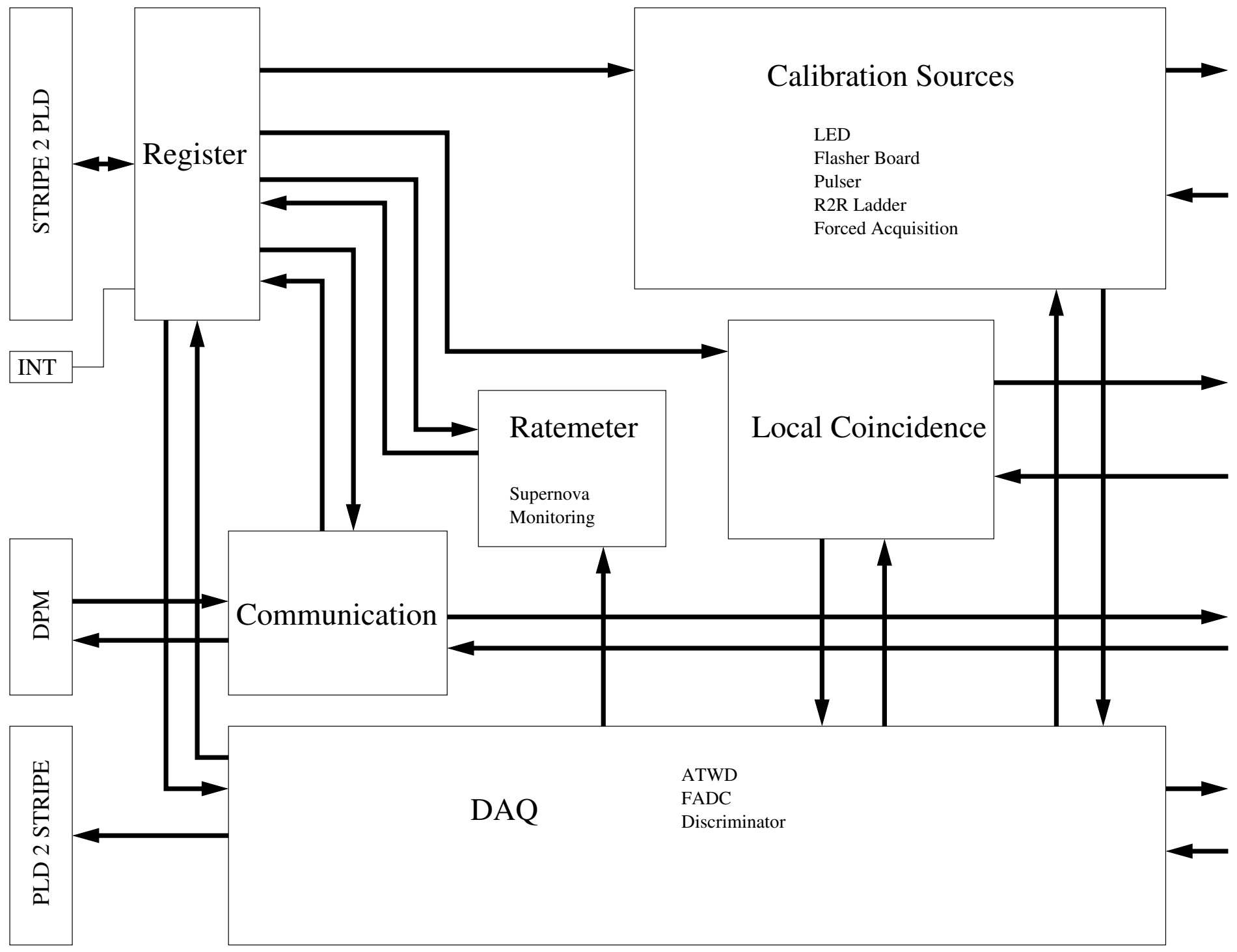


Figure 10

CPU

FPGA
External
Hardware



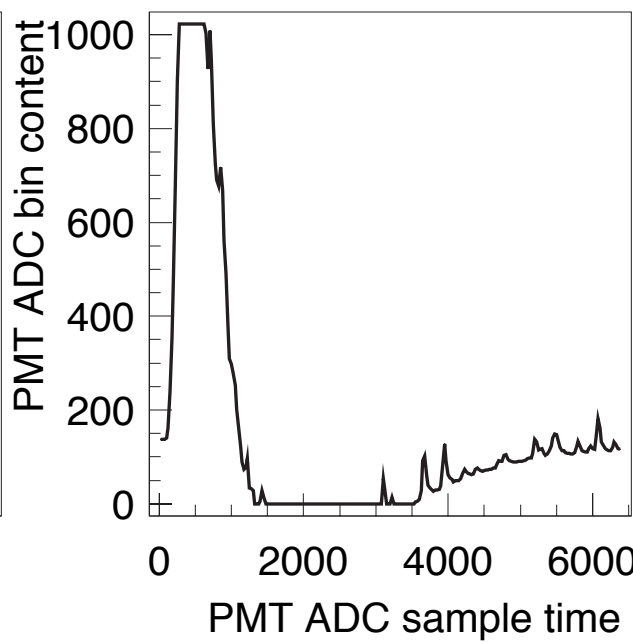
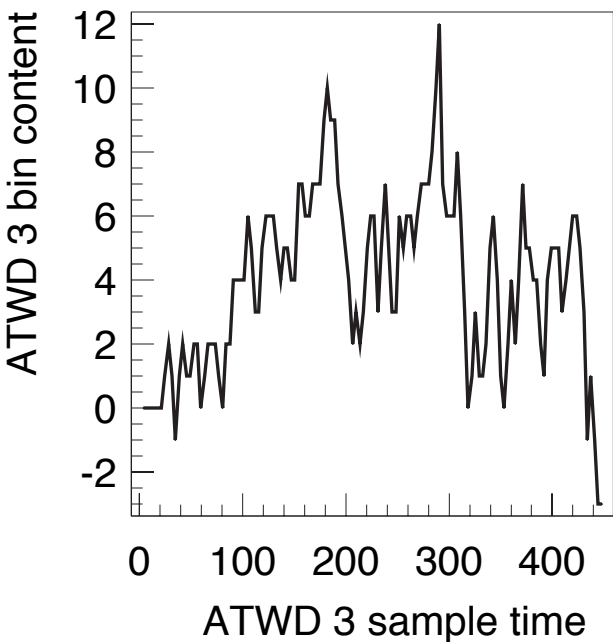
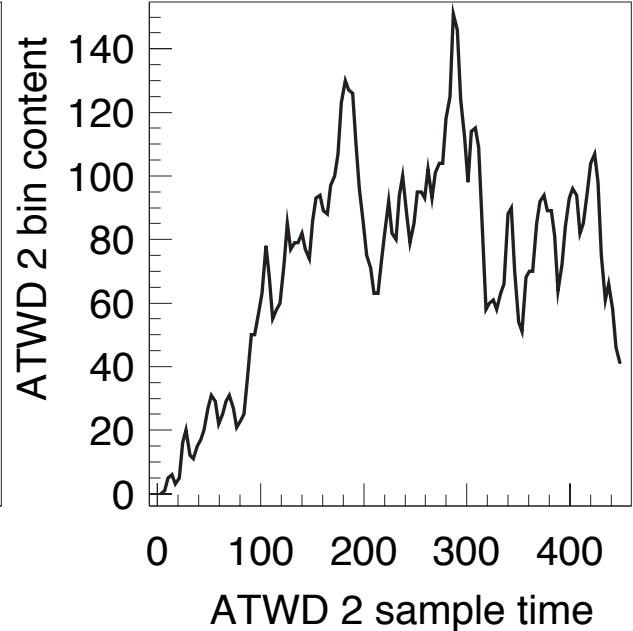
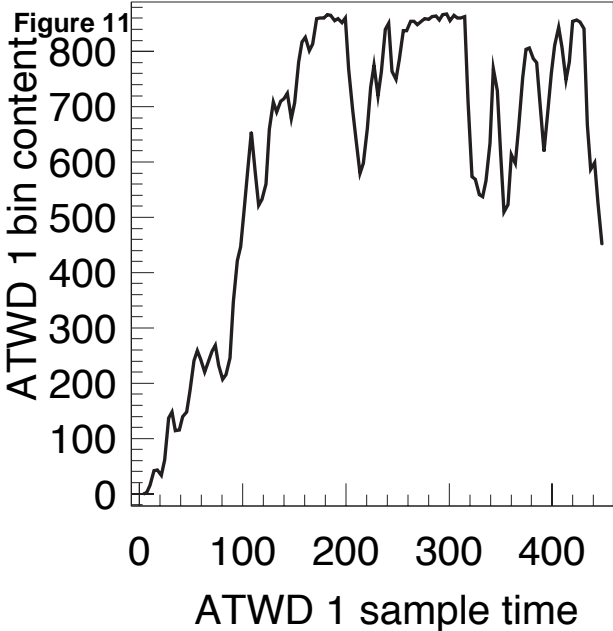


Figure 12

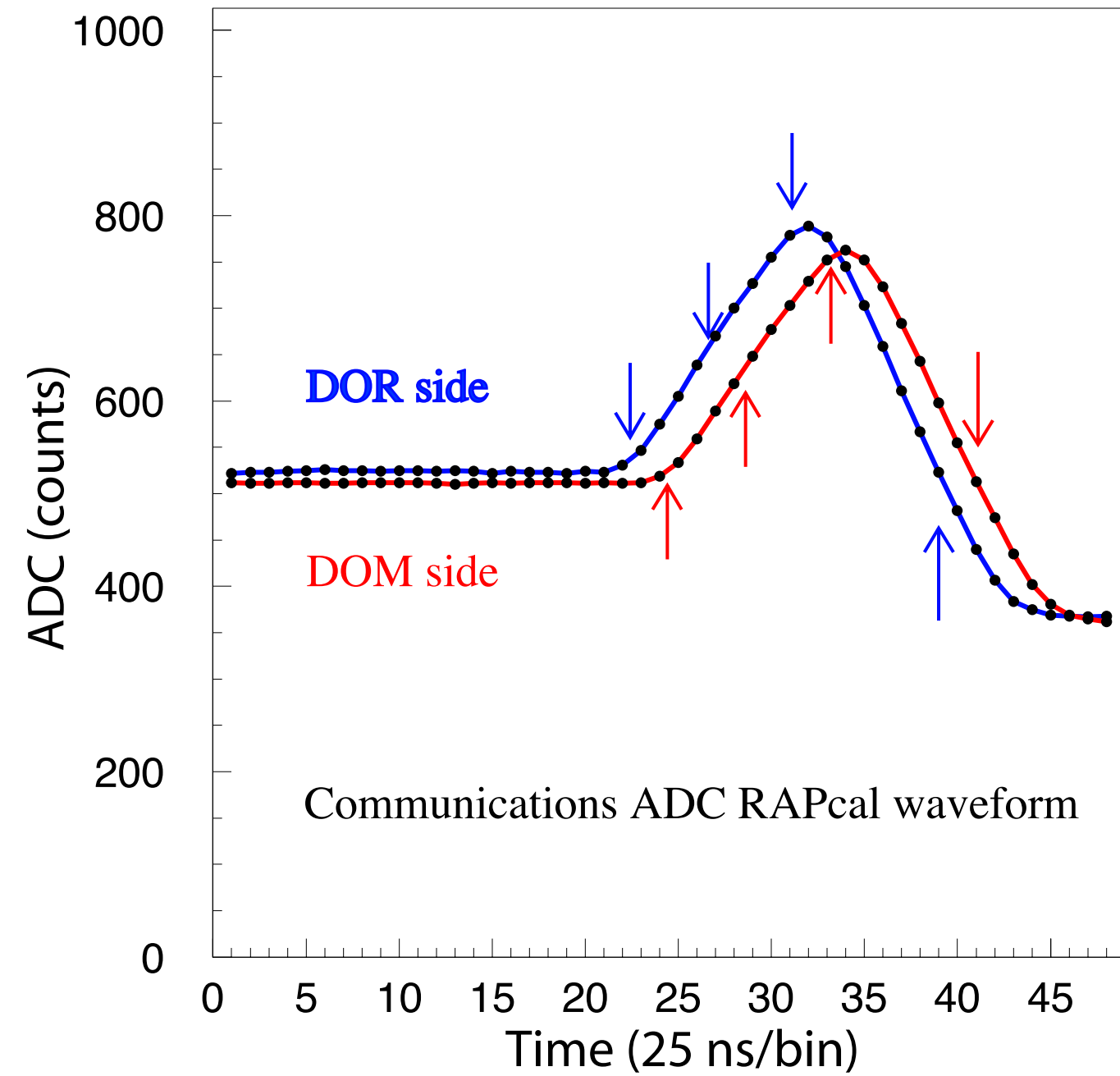


Figure 13

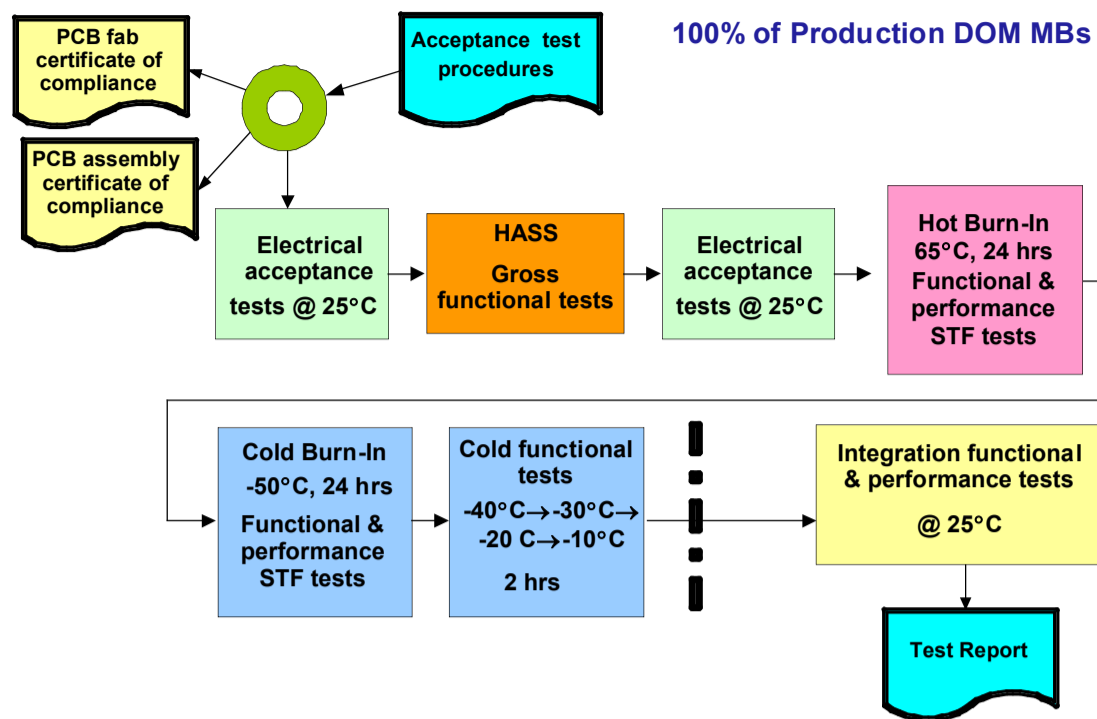


Figure 14
[Click here to download high resolution image](#)

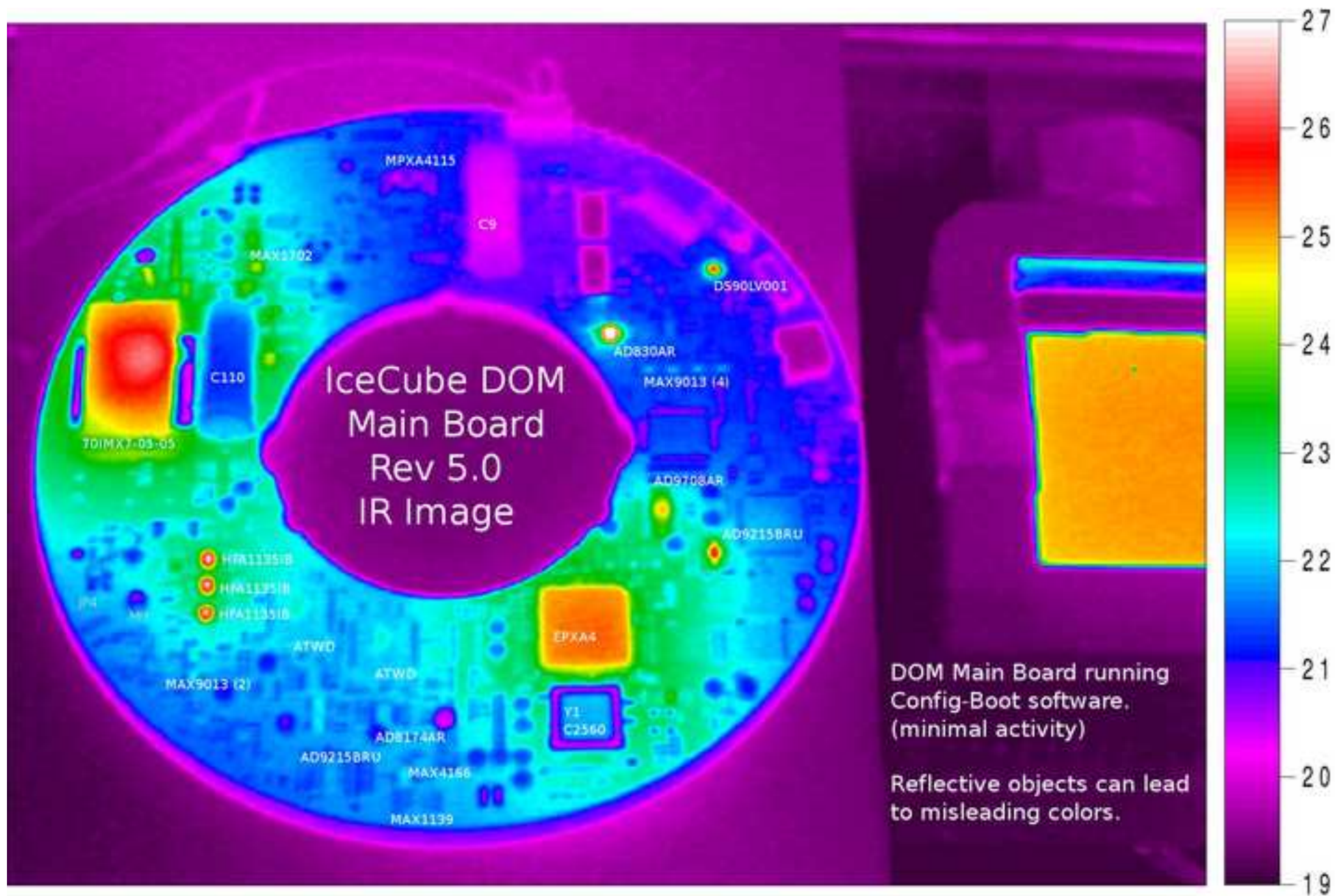


Figure 15

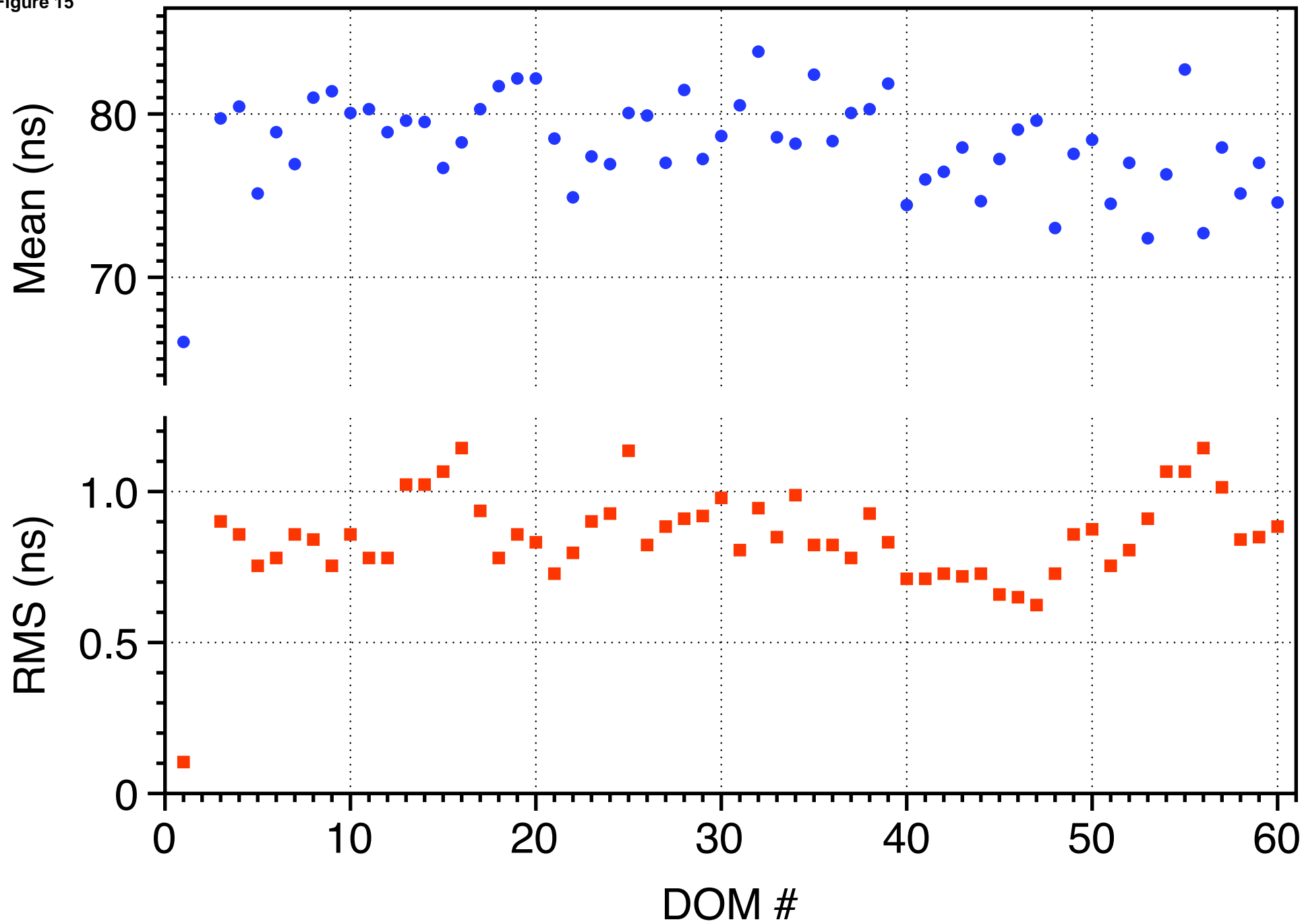
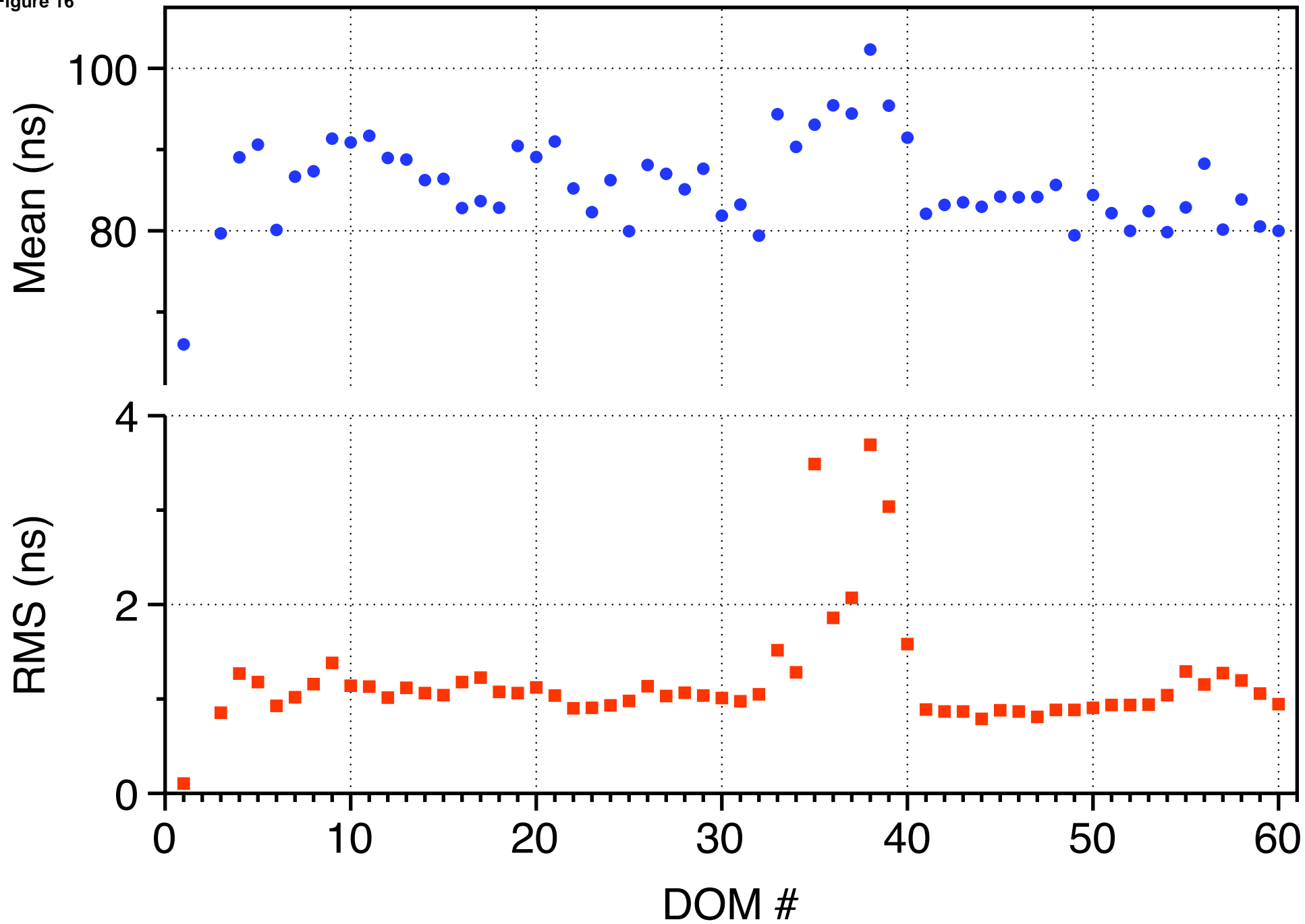


Figure 16



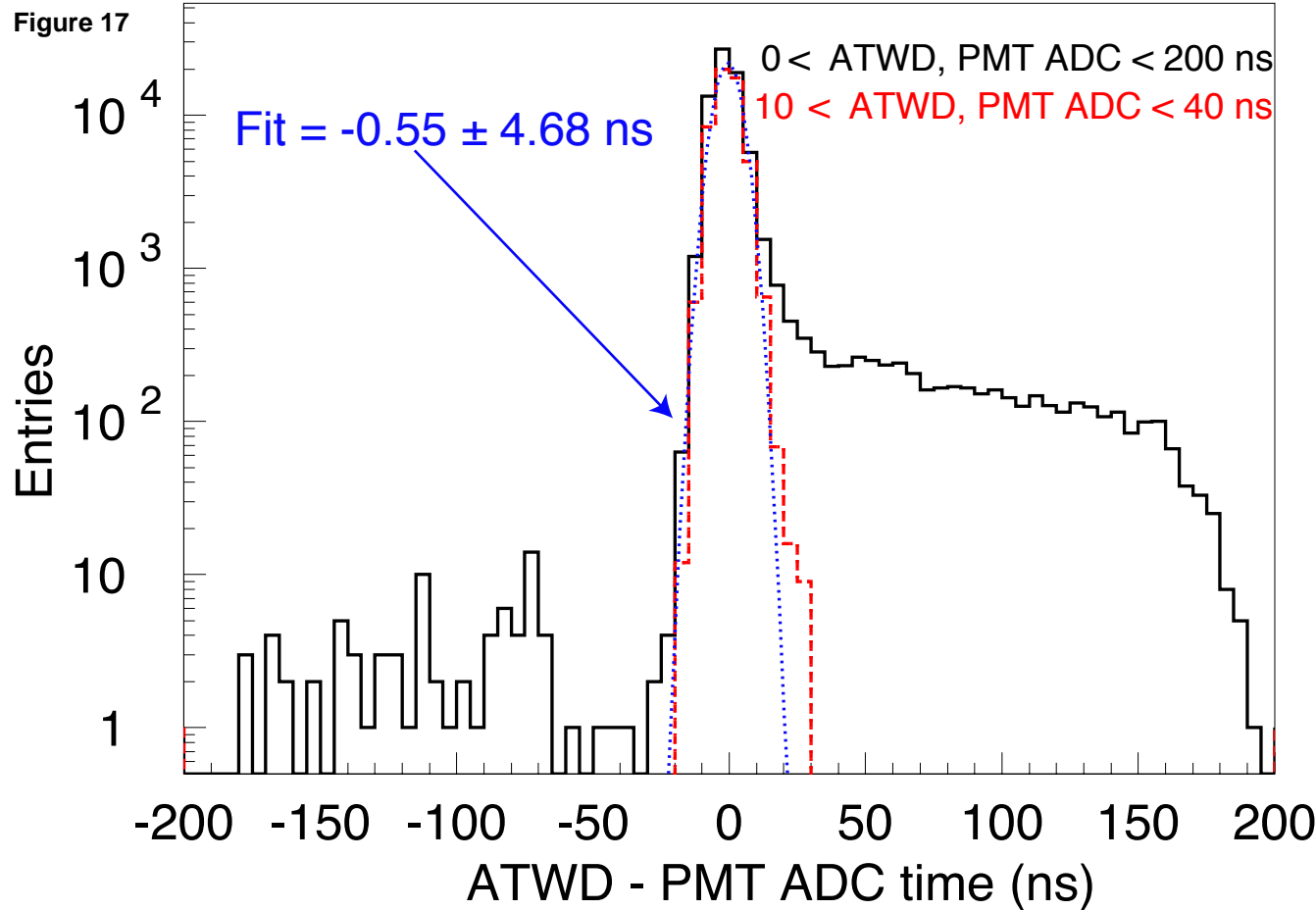


Figure 18

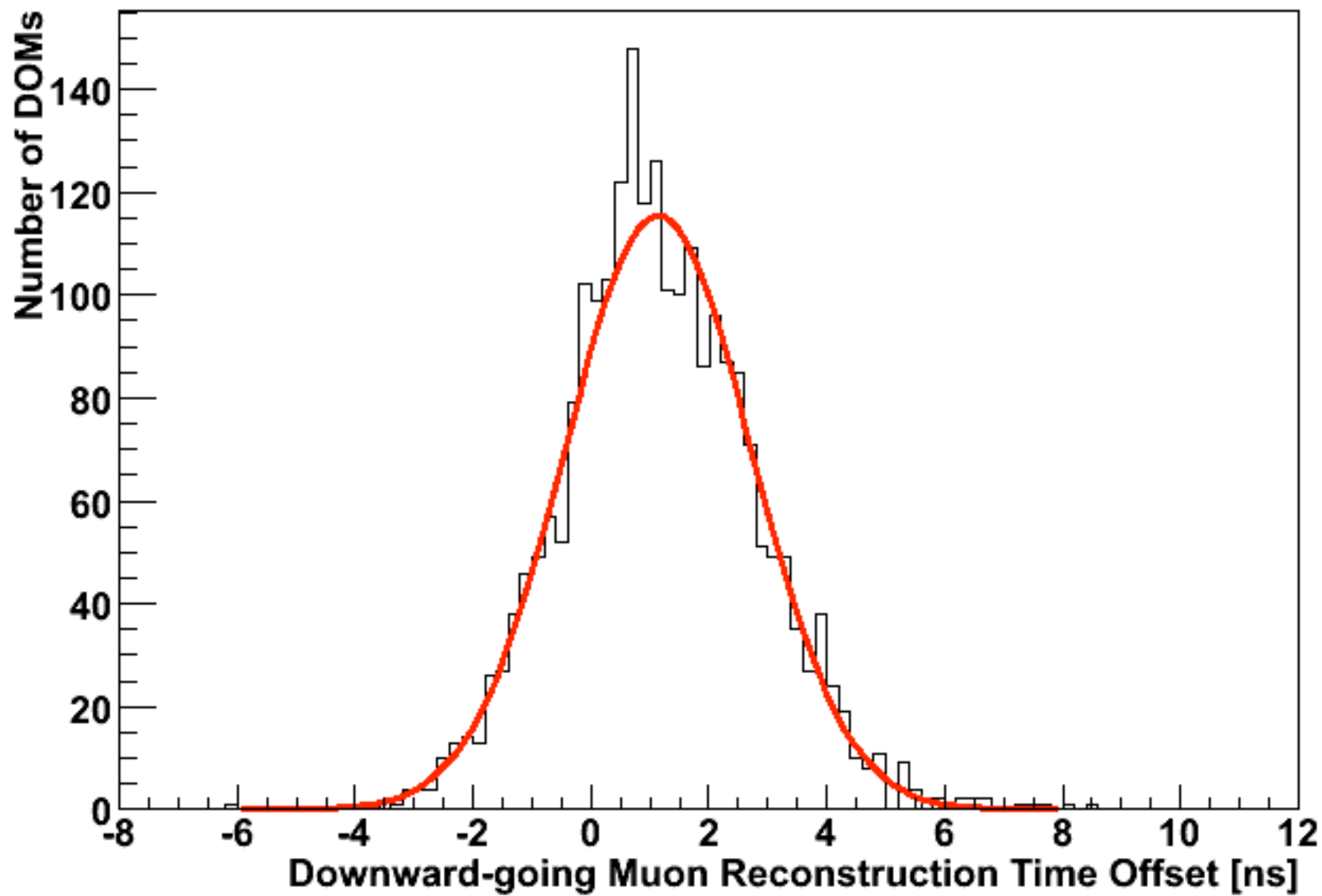


Figure 19

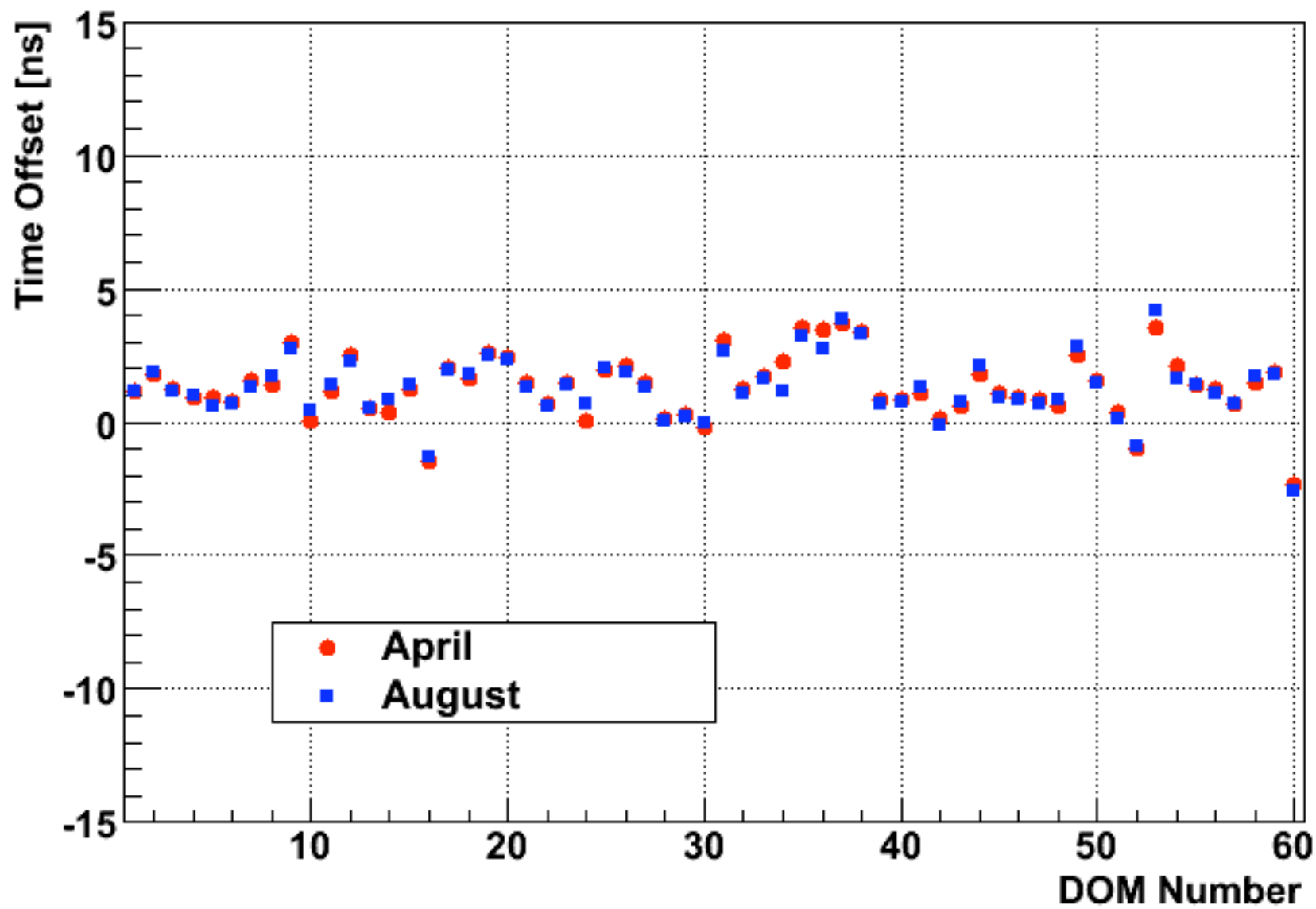


Figure 20

